

---

# SKIN-R1: TOWARD TRUSTWORTHY CLINICAL REASONING FOR DERMATOLOGICAL DIAGNOSIS

---

A PREPRINT

<b>Zehao Liu</b> Pennsylvania State University zml5418@psu.edu	<b>Wejeying Ren</b> Stanford University wjyren@stanford.edu	<b>Jipeng Zhang</b> Hong Kong University of Science and Technology jzhanggr@connect.ust.hk
<b>Tianxiang Zhao</b> Pennsylvania State University txiangchao@gmail.com	<b>Jingxi Zhu</b> Pennsylvania State University jqz5678@psu.edu	<b>Xiaoting Li</b> Pennsylvania State University xiaotili0123@gmail.com
	<b>Vasant G. Honavar</b> Pennsylvania State University vuh14@psu.edu	

## ABSTRACT

The emergence of vision-language models (VLMs) has opened new possibilities for clinical reasoning and has shown promising performance in dermatological diagnosis. However, their trustworthiness and clinical utility are often limited by three major factors: (1) Data heterogeneity, where diverse datasets lack consistent diagnostic labels and clinical concept annotations; (2) Absence of grounded diagnostic rationales, leading to a scarcity of reliable reasoning supervision; and (3) Limited scalability and generalization, as models trained on small, densely annotated datasets struggle to transfer nuanced reasoning to large, sparsely-annotated ones.

To address these limitations, we propose Skin-R1, a novel dermatological VLM that combines deep, textbook-based reasoning with the broad generalization capabilities of reinforcement learning (RL). Skin-R1 systematically resolves the key challenges through a unified, end-to-end framework. First, we design a textbook-based reasoning generator that synthesizes high-fidelity, hierarchy-aware, and differential-diagnosis (DDx)-informed trajectories, providing reliable expert-level supervision. Second, we leverage the constructed trajectories for supervised fine-tuning (SFT) empowering the model with grounded reasoning ability. Third, we develop a novel RL paradigm that, by incorporating the hierarchical structure of diseases, effectively transfers these grounded reasoning patterns to large-scale, sparse data. Extensive experiments on multiple dermatology datasets demonstrate that Skin-R1 achieves superior diagnostic accuracy. The ablation study demonstrates the importance of the reasoning foundation instilled by SFT.

## 1 Introduction

Every year, millions of people worldwide suffer from delayed or incorrect assessments of conditions such as melanoma, eczema, and psoriasis—often due to limited access to dermatologists Hay et al. [2014], Feng et al. [2018], Resneck Jr and Kimball [2004] or subjective interpretation of visual symptoms. Advances in computer vision, deep learning, and multimodal data integration now offer the possibility of AI-assisted systems to analyze dermoscopic and clinical images with expert-level precision, supporting clinicians in triage, screening, and treatment planning. By combining human expertise with AI, AI-assisted dermatology promises to democratize high-quality skin care and reduce the global burden of preventable dermatological disease Zhou et al. [2024], Liu et al. [2020], Cruz-Roa et al. [2013], Yuan et al. [2017].

Despite the notable performance gains achieved by recent multimodal vision foundation models geared toward dermatology and Med-VLMs [Yan et al., 2025a, Kim et al., 2024, Yan et al., 2025b, Koh et al., 2020, Yan et al., 2023,

Table 1: Comparison of representative Medical VLMs in terms of key diagnostic reasoning abilities. **Grounded Rationale** measures the ability to generate clinically faithful explanations consistent with real diagnostic principles; **DDx Awareness** reflects awareness of differential diagnoses through comparative reasoning; **Hierarchical Awareness** captures understanding of disease taxonomy and multi-level relations; and **Sparse-Supervision Learning** measures the ability to learn and generalize from sparsely annotated data.

Type	Model	Grounded Rationale	DDx Awareness	Hierarchical Awareness	Sparse-Supervision Learning
RL-based	Med-R1 [Lai et al., 2025]	✗	✗	✗	✓
	MedVLM-R1 [Pan et al., 2025]	✗	✗	✗	✓
	MedCCO [Rui et al., 2025]	✗	✗	✗	✓
	RARL [Pham and Ngo, 2025]	RL reward	✗	✗	✓
	Zhu et al. [2025a]		✗	✗	✓
SFT-based	MM-Skin [Zeng et al., 2025]	grounding SFT	✗	✗	✗
	OmniV-Med [Jiang et al., 2025]	grounding SFT	✓	✗	✗
	LLaVA-Med [Li et al., 2023]	distillation	✓	✗	✗
	HuatuGPT-Vision [Chen et al., 2024]	distillation	✓	✗	✗
Hybrid	MedGemma [Sellergren et al., 2025]	grounding SFT, distillation, RL reward	✓	✗	✓
	<b>Skin-R1</b>	<b>grounding SFT</b>	<b>✓</b>	<b>✓</b>	<b>✓</b>

Hu et al., 2024a], they suffer from significant limitations. Existing methods, such as SkinGPT-4 [Zhou et al., 2024], rely on labor-intensive human annotations and lack clinically grounded diagnostic rationales.

Building a reliable dermatology VLM presents three major challenges: (1) **Data heterogeneity**. Real-world datasets differ widely in diagnostic ontologies and concept vocabularies. For example, SkinCon [Daneshjou et al., 2022] annotated 29 dermatological concepts (e.g., Erythema, Plaque) but provides only two broad diagnoses: benign and malignant, while DermNet [der] includes images spanning more than 600 fine-grained diseases but lacks concept annotations, leading to inconsistent and noisy data. (2) **Lack of expert-like reasoning supervision**. Reliable diagnosis requires reasoning that respects hierarchical taxonomies and supports differential diagnosis (DDx), yet such structured reasoning signals are rarely available in existing datasets. (3) **Limited scalability of training paradigms**. Models trained on small, densely annotated data often fail to generalize to large, sparsely labeled datasets, making it difficult to transfer grounded diagnostic reasoning at scale.

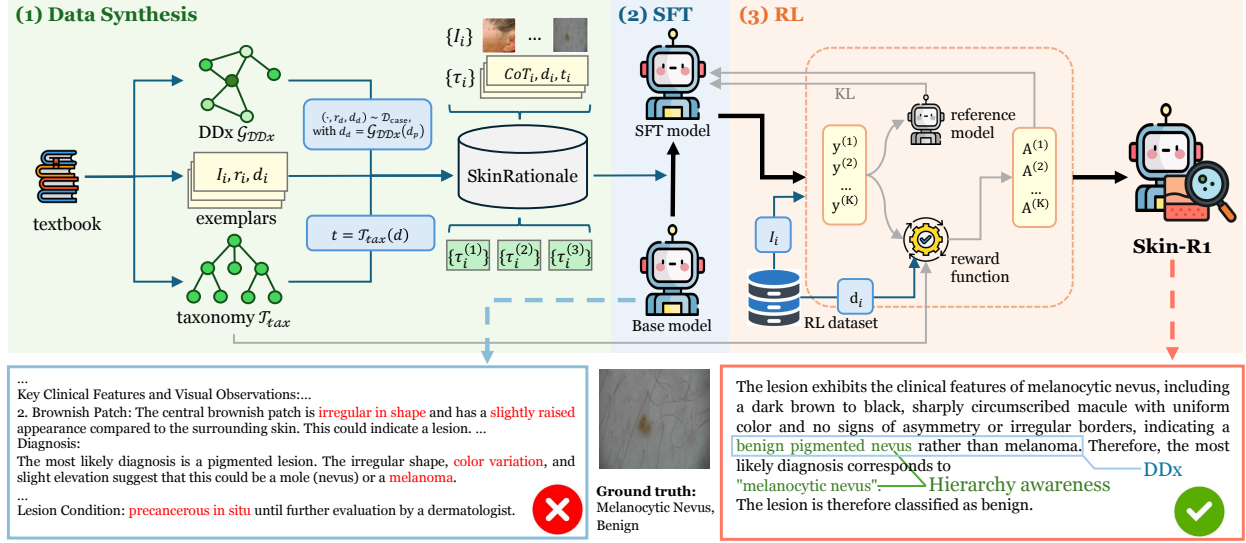
These challenges define the central problem this paper addresses: how to develop a dermatological VLM that embeds expert-like reasoning, incorporating both diagnostic hierarchies and DDx, for reliable and accurate diagnosis, yet remains scalable to large, heterogeneous datasets with sparse annotations. This requires a framework that can first acquire these grounded reasoning patterns from a reliable source and then effectively generalize them.

To address these challenges, we propose Skin-R1, which, to the best of our knowledge, is the first dermatology-oriented VLM that integrates deeply grounded clinical reasoning derived from textbook knowledge and further adapts it to the task through reinforcement learning. Skin-R1 unifies expert-aligned reasoning and scalable knowledge transfer into a single, end-to-end framework. To ensure reliable, expert-aligned reasoning, we assemble a grounded data set, consisting of hierarchy-aware and DDx-informed diagnostic trajectories based on authoritative textbook knowledge. Second, to build grounded reasoning foundation functioning as a warm for large-scale RL training, we perform supervised fine-tuning leveraging constructed trajectory data, enabling the model to perform clinically consistent reasoning. Third, to scale up this reasoning capacity, we design an RL-based training framework guided by hierarchical diagnostic accuracy and structured output regularization rewards. This framework encourages the model to spontaneously generalize its previously learned grounded diagnostic reasoning ability to large-scale sparsely-annotated data.

Our main contributions can be summarized as follows: (1) We introduce Skin-R1, a novel end-to-end framework for dermatology VLMs that unifies deep, textbook-grounded reasoning with a scalable, RL-based generalization strategy to leverage heterogeneous and sparsely-annotated data. (2) We design a textbook-grounded reasoning trajectory generator that synthesizes hierarchy-aware and DDx-informed reasoning traces, providing a scalable source of high-quality supervision for clinical reasoning. (3) We develop a novel RL paradigm for diagnostic models that aligns with real-world clinical scenarios by incorporating the hierarchical structure of diseases. This approach effectively transfers reliable reasoning patterns from dense data to sparse large-scale data. (4) We present the results of extensive experiments with multiple dermatology data sets which show that Skin-R1 outperforms state-of-the-art (SOTA) baselines on metrics that assess and diagnostic accuracy and robustness.

## 2 Related Work

**Medical Vision Large Language Models.** Visual language models (VLMs) [Bai et al., 2025, Liu et al., 2023, Zhu et al., 2023, Yin et al., 2023, Awais et al., 2025] extend the question-answering capabilities of LLMs [OpenAI, 2023, Touvron et al., 2023, Team et al., 2023] to the visual domain. Med-VLMs [Ren et al., 2025, Zhou et al., 2023, Tian



et al., 2024] further extend LLMs to clinical applications by (1) developing medical foundation models (MFMs) as domain-specific visual backbones, (2) integrating medical visual encoders with large language models, and (3) scaling multimodal alignment across diverse clinical data modalities.

Early efforts aimed at improving the visual ability of LLMS in medical scenarios focused on developing medical foundation models in subdomains such as radiology [Wang et al., 2022], pathology [Lu et al., 2024], and dermatology [Yan et al., 2025a, Kim et al., 2024, Yan et al., 2025b]. To equip Med-VLMs with clinically grounded visual reasoning, subsequent works adopted an encoder-decoder paradigm, such as XrayGPT [Thawkar et al., 2023] integrating Med-CLIP [Wang et al., 2022] with a fine-tuned LLM. LLaVA-Med [Li et al., 2023] leverages PubMed image-text pairs to enhance cross-modal alignment. BiomedGPT [Luo et al., 2024] adopts a BERT-GPT hybrid architecture trained on biomedical corpora; and HuatuoGPT-Vision [Chen et al., 2024] adopts a similar architecture trained on the large-scale PubMedVision dataset. To bridge the gap between understanding and generation of medical images, HealthGPT [Lin et al., 2025] unifies both tasks within a single autoregressive token-prediction framework. To further advance the understanding of dermatological images and diagnostic reasoning, SkinGPT-4 [Zhou et al., 2024] adopts a two-step medical instruction-tuning framework.

Despite these remarkable achievements, most existing Med-VLMs require vast amounts of high-quality data, which limits their applicability in domains with limited expert-curated annotations. In contrast, Skin-R1 leverages a small set of high-quality grounded data to establish a solid reasoning foundation and then uses RL to efficiently transfer and expand diagnostic reasoning capabilities.

**RL-Driven Emergence of Reasoning Abilities on Med-VLMs.** Recent advances in reinforcement learning (RL) for LLMs and VLMs [Guo et al., 2025, Xie et al., 2025, Chen et al., 2025, Hu et al., 2025, Zhang et al., 2025] have shown that such models can mimic reasoning when trained with carefully designed RL objectives with Verifiable Rewards (RLVR). DeepSeek-R1 [Guo et al., 2025] extended RLVR using Group Relative Policy Optimization (GRPO) to large models, exhibiting emergent reasoning without the need for explicit chain-of-thought (CoT) supervision.

RL has also been used successfully to improve the reasoning ability of Med-VLMs on diagnostic tasks [Lai et al., 2025, Pan et al., 2025, Rui et al., 2025, Pham and Ngo, 2025, Zhu et al., 2025a]. Due to the scarcity of high-quality annotated data, these approaches typically bypass the SFT stage and perform RL directly via GRPO. This RL-only paradigm has shown substantial improvement in medical visual question answering and generalization across data modalities.

MedVLM-R1 [Pan et al., 2025] has shown that GRPO can induce emergent CoT reasoning without explicit reasoning supervision, thus improving model generalization. As discussed in Med-R1 [Lai et al., 2025], conventional SFT often suffers from *memorization shortcuts*, and in some cases, models trained without explicit reasoning supervision (e.g., No-Thinking-Med-R1) even outperform those with CoT-based RL training. We argue that this phenomenon arises from the lack of clinically grounded and textbook-based reasoning data, leading to heuristic, partial, or even hallucinated rationales [Lanham et al., 2023, Huang et al.].

In contrast, Skin-R1 directly addresses this limitation by first providing expert-like diagnostic reasoning patterns through a small set of high-quality diagnostic trajectories and then employing RL to amplify and generalize this grounded reasoning. Ablation experiments (see section 4.2) empirically validate the effectiveness of such grounded reasoning instilled by SFT.

### 3 Methods

Skin-R1, is designed to address the unique challenges of building trustworthy dermatological VLMs by establishing a robust multi-stage training pipeline. This pipeline systematically progresses from synthesizing high-quality textbook-grounded reasoning data to fine-tuning and generalizing the model’s diagnostic capabilities. First, we detail the construction of SkinRationale, a novel data set that explicitly captures multi-step, hierarchy-aware, and differential diagnosis (DDx)-informed reasoning trajectories from authoritative dermatology references. Subsequently, we present our two-stage training methodology: Supervised Fine-Tuning (SFT) on SkinRationale to instill a foundational understanding of grounded reasoning, followed by Reinforcement Learning (RL) via Group-Relative Policy Optimization (GRPO) to enhance the model’s generalization and robustness across diverse, sparsely-annotated clinical datasets.

#### 3.1 Training Data for Grounded Reasoning

To enable trustworthy and evidence-based dermatological diagnostic reasoning, it is essential to develop resources that can elicit multi-step reasoning and clinically meaningful trajectories. However, existing dermatology datasets primarily focus on visual classification or lesion segmentation and lack detailed annotations that explicitly link visual concepts to diagnostic results. In addition, they rarely include diagnostic rationales, leaving the reasoning process between observed features and clinical conclusions unmodeled. To address these limitations, we introduce SkinRationale, a textbook-based data set derived from authoritative dermatology references.

##### 3.1.1 Extracting Textbook Grounded Exemplar

We begin by systematically extracting the corresponding diagnosis of each image and its diagnostic rationale from curated clinical textbooks. Each exemplar is represented as a triplet, i.e.,  $\mathcal{D} = (I_i, r_i, d_i)_{i=1}^N$ , where  $I_i$  denotes a clinical image,  $r_i$  is the textual rationale describing the evidence and reasoning behind the diagnosis, and  $d_i$  is the diagnostic label.

##### 3.1.2 Constructing Reasoning Trajectories

After extracting diagnostic exemplars, the next challenge lies in generating reliable solution trajectories for cold-start supervision. Although open-source Large Reasoning Models (LRMs) such as QwQ-32B Team [2025] can produce partially correct reasoning traces, directly using their outputs for fine-tuning can result in model collapse [Shumailov et al., 2024] and hallucination propagation [Wang et al., 2025]. We identify two key challenges. (1) Inconsistency of the label granularity: the same lesion can be annotated at different levels of diagnostic specificity (e.g. melanoma vs. superficial spreading melanoma), creating ambiguity in supervision. (2) Ambiguity of differential diagnosis: dermatological reasoning requires not only identifying the correct disease but also explicitly ruling out alternatives that share similar visual features. To address the two challenges, we introduce two complementary mechanisms that encode domain-specific diagnostic knowledge and enrich reasoning supervision.

**Hierarchical diagnosis completion.** We construct a dermatology diagnosis tree that captures parent–child relationships among disease entities (e.g., melanoma → superficial spreading melanoma). We augment each final label by adding its ancestral and sibling nodes. This process mitigates inconsistency in the granularity of labels and enforces taxonomic coherence, enabling the model to learn shared representations across coarse and fine-grained diagnostic categories.

**Differential diagnosis reasoning enrichment.** We further build a differential diagnosis (DDx) graph from authoritative dermatology textbooks, encoding relationships among clinically confusable conditions (e.g., pigmented nevus vs.

melanoma). During trajectory synthesis, this graph guides the generation of differential-aware rationales, injecting explicit reasoning chains that articulate how similar diseases are differentiated or ruled out. By integrating these rationales informed by DDx into the trajectories, the model learns to identify the correct diagnosis and to provide an interpretable justification for excluding alternatives.

The trajectories are organized as

$$\{\tau_i\}_{i=1}^K = \{(CoT_i, d_i, t_i)\}_{i=1}^K, \quad (1)$$

where each trajectory consists of a clinically grounded rationale  $CoT_i$ , a disease label  $d_i$ , and expanded hierarchical diagnostic information  $t_i$ . The hierarchy-aware and DDx-informed diagnostic trajectories design enables SkinRationale to represent multi-level diagnostic reasoning that mirrors the decision processes of dermatologists. Details of trajectory synthesis are provided in Appendix section B.

### 3.2 Enhancing Grounded Medical Reasoning

To build a grounded reasoning foundation for the model, we first leverage SkinRationale for SFT, instilling the model with reliable reasoning foundation. Subsequently, we employ RL to generalize this reasoning ability to sparsely-annotated dermatology datasets.

#### 3.2.1 Supervised Fine-Tuning on SkinRationale.

To capture grounded reasoning trajectories for dermatological diagnosis, we train the policy model  $\pi_\theta$  through SFT on hierarchy-aware and DDx-informed diagnostic trajectories. Given a clinical image  $I$ , an instruction prompt  $p$  and the complete diagnostic trajectory  $\tau = (x_0, x_1, \dots, x_{n-1}, x_n)$ , the objective loss function  $L$  is formulated as follows:

$$L = - \sum_{i=1}^n \log \pi_\theta(x_i \mid x_{<i}, I, p), \quad (2)$$

This objective enables the policy to imitate expert trajectories across the hierarchical diagnostic space, integrating reflective reasoning with structured clinical decision making, and thus establishing a robust foundation for RL fine-tuning.

#### 3.2.2 Reinforcement Learning via GRPO

While SFT on trajectory instills the ability of expert-style reasoning, it is primarily confined to the given trajectories. To scale this capability and generalize it to large-scale, sparsely-annotated real-world datasets, the final stage reformulates the diagnostic task as a RL problem. This stage utilizes Group-Relative Policy Optimization (GRPO) [Shao et al., 2024] to effectively generalize the model’s clinically-grounded diagnostic reasoning policies, even when explicit reasoning supervision is unavailable. Unlike conventional PPO [Schulman et al., 2017] or DPO [Rafailov et al., 2023], GRPO leverages relative advantages within groups of sampled responses instead of absolute reward, enabling stable, value-free policy refinement.

Given an input sample  $x = (I, q)$ , the policy  $\pi_\theta$  generates  $K$  candidate responses

$$\{y^{(j)}\}_{j=1}^K = \{(CoT^{(j)}, \hat{\ell}^{(j)}, \hat{b}^{(j)})\}_{j=1}^K, \quad (3)$$

where each candidate comprises a reasoning process  $CoT^{(j)}$ , a predicted disease label  $\hat{\ell}^{(j)}$ , and a predicted lesion condition  $\hat{b}^{(j)}$ . Each  $y^{(j)}$  is evaluated using a designed reward  $r_j = R_{\text{total}}(\mathcal{P}, y^{(j)})$ , where  $R_{\text{total}}$  jointly measures diagnostic correctness and structural consistency, and  $\mathcal{P}$  denotes the ground-truth path in the hierarchical taxonomy of diagnoses. To ensure stable optimization, rewards are normalized within each group, expressed as  $A_j = (r_j - \mu)/\sigma$ , where  $A_j$  denotes the standardized advantage of  $y^{(j)}$ . The policy is updated via a clipped PPO-style objective, augmented with KL regularization toward the SFT reference policy  $\pi_{\text{ref}}$ :

$$\begin{aligned} \mathcal{L}_{\text{GRPO}}(\theta) = & \mathbb{E}_x \left[ \frac{1}{K} \sum_{j=1}^K \min \left( \rho_j A_j, \text{clip}(\rho_j, 1 - \varepsilon, 1 + \varepsilon) A_j \right) \right] \\ & - \beta \text{KL}(\pi_\theta(\cdot \mid x) \parallel \pi_{\text{ref}}(\cdot \mid x)), \end{aligned} \quad (4)$$

where  $\rho_j = \pi_\theta(y^{(j)} \mid x) / \pi_{\theta_{\text{old}}}(y^{(j)} \mid x)$  represents the importance ratio, and  $\beta$  regulates the strength of the KL penalty to balance exploration and policy retention. By reinforcing relatively superior responses within each group rather than absolute returns, GRPO eliminates the need for an explicit value function, achieving a stable and sample-efficient refinement of the model’s diagnostic reasoning policy.

**Reward function.** The reward function is formulated to incentivize diagnostic predictions that are structurally-valid, hierarchically-correct, and clinically-reliable, defined as:

$$R_{\text{total}} = R_{\text{format}} + R_{\text{gran}} + R_{\text{malignancy}}, \quad (5)$$

**Format Compliance Reward ( $R_{\text{format}}$ ).** To encourage the model to produce outputs in the desired structured format, we introduce a binary format reward to measure the format consistency of the generated completion to the required tag set (e.g., `<thinking>`, `</thinking>`, `<diagnosis>`, `</diagnosis>`). The reward is defined as

$$R_{\text{format}} = \begin{cases} 1, & \text{if all tags are present in } y, \\ 0, & \text{otherwise.} \end{cases} \quad (6)$$

**Granularity-wise Reward ( $R_{\text{gran}}$ ).** To capture reward signal across the hierarchical disease taxonomy as well as encourage the model to produce not only correct but also fine-grained diagnostic predictions, we introduce a granularity-aware reward that assigns higher values to correct finer-grained predictions. Given a ground-truth taxonomy path  $\mathcal{P} = [\ell_1, \ell_2, \dots, \ell_L] \subseteq \mathcal{T}_{\text{tax}}$ , where deeper levels correspond to finer-grained diagnoses, the model’s prediction  $\hat{\ell}$  is assumed to match one node along this path. For each level  $i$ , we define the normalized depth weight  $w_i = i/L$  and the indicator  $\delta_i = \mathbf{1}[\ell_i = \hat{\ell}]$ , the granularity-wise is then given by:

$$R_{\text{gran}} = 0.75 \cdot \sum_{i=1}^L w_i \cdot \delta_i = w_{i^*}, \text{ where } i^* \text{ is the depth of } \hat{\ell}. \quad (7)$$

Hence,  $R_{\text{gran}}$  increases with the granularity of the correct prediction, reaching its maximum of 0.75 when the finest-grained label  $\ell_L$  is correctly identified. This hierarchical formulation encourages progressive diagnostic refinement while preserving strict correctness guarantees.

**Malignancy Discrimination Reward ( $R_{\text{malignancy}}$ ).** Distinguishing between benign and malignant lesions is a fundamental clinical task, representing the most coarse-grained yet most critical diagnostic classification. To ensure the correctness of benign versus malignant diagnosis, we use  $R_{\text{malignancy}}$  to explicitly reinforce correct high-level predictions. Let  $b^* \in \{\text{benign, malignant, precancerous in situ}\}$  denote the ground-truth category, and  $\hat{b}$  the class predicted by the model. The reward is defined as a binary indicator:

$$R_{\text{malignancy}} = \begin{cases} 0.25, & \text{if } \hat{b} = b^*, \\ 0, & \text{otherwise.} \end{cases} \quad (8)$$

## 4 Experiments and Results

**Training & Testing Datasets.** We employ 6 dermatology datasets for RL training as well as test: PAD-UFES-20 [Pacheco and Krohling, 2020], DermNet [der], BCN20000 [Combalia et al., 2019], DERM12345 [Yilmaz et al., 2024], Derm7pt [Kawahara et al., 2019], and HAM10000 [Tschandl, 2018]. To assess generalization, we additionally evaluate the trained model on the dermoscopy subset of OmniMedVQA [Hu et al., 2024b]. Detailed descriptions of all datasets and dataset preprocessing are provided in Appendix section A.

**Task Description.** We design a comprehensive visual question answering (VQA) task to evaluate the comprehensive diagnostic capability of our model under multiple distributional scenarios. The task includes three settings: (1) **In-distribution disease diagnosis**, where the model predicts the disease category based on dermoscopic images within the training domain; (2) **Out-of-distribution (OOD) disease diagnosis**, which assesses the model’s generalizability to unseen disease types outside the training distribution. ; and (3) **In-distribution lesion condition diagnosis**, where the model classifies each case into one of three lesion conditions: benign, malignant, or precancerous *in situ*.

All tasks are formulated as multiple-choice VQA problems, evaluated primarily by accuracy. For the skin lesion diagnosis task, Macro F1 is additionally reported to address class imbalance. To ensure fair comparison, an answer extraction step is applied to baselines lacking the specified response format. Details of the multiple-choice setup are provided in Appendix section A

**Implementation Details.** We adopt Qwen2.5-VL-7B-Instruct [Bai et al., 2025] as the backbone model. Both SFT and RL stages are trained with the LoRA technique [Hu et al., 2022], using the following hyperparameters: `lora_r=64`, `lora_alpha=32`, and `lora_dropout=0.1`. More details of implementation are provided in Appendix section C.

Table 2: Comparison of Skin-R1 with baseline LVLMs on in-distribution and OOD disease diagnostic tasks. **Bold** and underlined values indicate the best and second-best results, respectively.

Type	Model	In-distribution						OOD						
		BCN20k	HAM10k	PAD	derm12345	derm7pt	dermnet	Avg.	ISBI16	ISIC18	ISIC19	ISIC20	Monk22	Avg.
General	Qwen2.5-VL-7B-Instruct	0.4911	<b>0.5162</b>	0.5033	0.3521	0.2962	0.4852	0.4367	0.3655	0.6301	0.6359	0.3325	<b>0.7078</b>	0.5027
	Qwen3-VL-8B-Instruct	0.2947	0.2085	0.3275	0.2386	0.2354	0.2899	0.2585	<u>0.6996</u>	0.2890	0.3934	<b>0.8837</b>	0.4610	0.5939
	InternVL3-8B	0.4996	0.4705	0.6009	0.3453	0.3364	0.5473	0.4430	0.4580	<u>0.6474</u>	<b>0.7746</b>	0.3531	0.6948	0.5841
	LLaVA-v1.6-7B	0.2299	0.2416	0.3080	0.3046	0.2354	0.2885	0.2636	0.5819	0.1908	0.3134	0.5899	0.3312	0.4351
	LLaVA-v1.6-13B	0.3933	0.3779	0.4469	<u>0.4121</u>	0.3376	0.4193	0.3960	0.2563	0.1676	0.3415	0.1584	0.2143	0.2560
	Qwen2.5-VL-32B-Instruct	0.4746	0.4057	0.4469	0.3815	<u>0.3596</u>	<b>0.5763</b>	0.4307	0.5966	0.2601	0.3445	0.6040	0.3247	0.4587
	Qwen3-VL-32B-Instruct	0.3156	0.2363	0.3688	0.2801	0.2536	0.3304	0.2892	<b>0.6996</b>	0.3353	0.5596	<u>0.8408</u>	0.6688	0.6651
Medical	LLaVA-Med-7b	0.2508	0.2091	0.2039	0.2503	0.2135	0.2870	0.2400	0.2542	0.2601	0.3928	<b>0.5314</b>	0.4545	0.4170
	HuatuoGPT-Vision-7B	0.4799	0.4944	0.4295	0.3638	0.2561	0.4719	0.4241	0.4202	0.5896	0.5657	0.4505	0.5779	0.5101
	MedGemma-4B	0.4130	0.2627	0.3753	0.3767	0.2924	0.3240	0.3548	0.5168	0.5318	0.7214	0.7508	0.5584	<u>0.6887</u>
Dermatology	SkinVL-PubMM	-	-	-	-	-	-	-	-	-	-	-	-	-
	<b>Skin-R1</b>	<b>0.6345</b>	<b>0.7214</b>	<b>0.6573</b>	<b>0.6608</b>	<b>0.4955</b>	0.5370	<b>0.6385</b>	0.6828	<b>0.7630</b>	<b>0.7630</b>	0.6708	0.6494	<b>0.7171</b>

Table 3: Comparison of Skin-R1 with baseline LVLMs on in-distribution skin lesion diagnostic tasks. **Bold** and underlined values indicate the best and second-best results, respectively.

Type	Model	In-distribution						OOD						Avg.	
		BCN20k		HAM10k		PAD		Derm12345		Derm7pt		DermNet		Avg.	
		Acc	F1	Acc	F1	Acc	F1	Acc	F1	Acc	F1	Acc	F1	Acc	F1
General	Qwen2.5-VL-7B-Instruct	0.4308	0.3346	0.2905	0.2449	0.4100	0.3632	0.3046	0.2045	0.3661	0.3468	0.5399	0.4390	0.3698	0.2910
	Qwen3-VL-8B-Instruct	0.4581	0.3105	0.6592	0.3601	0.3124	0.2891	0.7437	0.3716	0.6494	<u>0.5858</u>	0.5059	0.3503	0.5924	0.3649
	InternVL3-8B	0.4795	<b>0.3768</b>	0.3514	0.2639	<u>0.5033</u>	<b>0.4932</b>	0.4769	0.3091	0.4334	0.4343	<b>0.5932</b>	<b>0.5366</b>	0.4619	0.3610
	LLaVA-v1.6-7B	0.4014	0.3036	0.5897	<u>0.3669</u>	0.2907	0.2743	0.6414	0.3285	0.5356	0.5361	0.4601	0.3109	0.5174	0.3428
	LLaVA-v1.6-13B	0.3704	0.3070	0.4057	0.2888	0.3536	0.3458	0.3847	0.2330	0.3739	0.4181	0.4267	0.3524	0.3849	0.2978
	Qwen2.5-VL-32B-Instruct	0.4799	0.3507	0.4917	0.3390	0.3514	0.3027	0.6093	0.3442	0.4903	0.4948	0.5896	0.4511	0.5231	<u>0.3654</u>
	Qwen3-VL-32B-Instruct	0.4481	0.2452	<u>0.7598</u>	0.3508	0.2560	0.1968	0.8716	<u>0.3923</u>	0.6986	0.4991	0.5333	0.3092	0.6491	0.3337
Medical	LLaVA-Med-7b	0.4465	0.2058	<b>0.7968</b>	0.2956	0.2299	0.1246	<b>0.8994</b>	0.3157	0.6986	0.4113	0.5459	0.2354	<b>0.6631</b>	0.2714
	HuatuoGPT-Vision-7B	0.4489	<u>0.3525</u>	0.3349	0.2858	<b>0.5098</b>	0.4725	0.3682	0.2390	0.3842	0.3957	0.5562	0.4680	0.4105	0.3267
	MedGemma-4B	0.0817	0.0746	0.0668	0.0558	0.3384	0.2302	0.0692	0.0574	0.0517	0.0813	0.1746	0.1531	0.0942	0.0816
Dermatology	SkinVL-PubMM	0.4368	0.2373	0.7187	0.3459	0.2560	0.1733	0.8740	0.3196	0.6779	0.5491	0.5592	0.2816	0.6392	0.3100
	<b>Skin-R1</b>	<b>0.5370</b>	0.3486	0.7472	<b>0.4039</b>	0.3536	0.2888	0.8918	<b>0.4786</b>	<b>0.7089</b>	<b>0.6589</b>	<b>0.6257</b>	0.4271	<b>0.6928</b>	<b>0.4287</b>

**Baselines.** We compare Skin-R1 with a diverse set of recent VLMs, covering both general-purpose and medical-domain foundations, as well as a dermatology-specific VLM. More specifically, our baselines include general-purpose VLMs such as Qwen2.5-VL-7B and -32B [Bai et al., 2025], Qwen3-VL-8B and -32B [Qwen AI / Alibaba Cloud, 2025], InternVL3-8B [Zhu et al., 2025b], and LLaVA-v1.6-7B and -13B [Liu et al., 2024]; medical VLMs including LLaVA-Med-7B [Li et al., 2023], HuatuoGPT-Vision-7B [Chen et al., 2024], and MedGemma-4B [Sellergren et al., 2025]; and a dermatology-focused VLM, SkinVL-PubMM [Zeng et al., 2025]. Furthermore, the Med-R1 [Lai et al., 2025] and MedVLM-R1 [Pan et al., 2025] training strategies mainly rely on pure GRPO with RLVR-style rewards. Thus, the **RL without SFT** setup in section 4.2 can be viewed as their adaptation to dermatology.

#### 4.1 Skin-R1 Compared with SOTA Benchmarks

As shown in table 2, **Skin-R1 significantly outperforms all baseline models in disease diagnosis**. It achieves the highest average accuracy on both in-distribution (ID) data (0.6385, an improvement of +0.1955 over the next-best model) and out-of-distribution (OOD) data (0.7171, +0.0284), demonstrating its superior accuracy and strong generalization capabilities. As shown in table 3, **Skin-R1 yields the most robust and balanced performance in the lesion condition diagnosis task**. It attains both the highest average accuracy (0.6928, +0.0297) and the highest average F1 score (0.4287, +0.0633).

Several baseline models show notable shortcomings. MedGemma-4B shows a strong bias that it almost exclusively to the rare C: *precancerous in situ* class (7,860 of 8,390 predictions), resulting in the worst performance. LLaVA-Med-7B shows a strong bias for the majority-class A: *benign* (5,563 of 8,390 predictions), leads to poor F1 scores. SkinVL-PubMM also shows a mild bias toward the A: *benign* class. Moreover, on both ID and OOD diagnostic tasks, SkinVL-PubMM rarely produces valid responses, even when the prompts are adaptively simplified, and its metrics are therefore marked as with “-”.

#### 4.2 Ablation Study

We summarize the results of an ablation study to evaluate the impact of SFT on trajectories, RL checkpoints at different stages, and the effect of removing SFT (**RL without SFT**) in table 4 and table 5.

Table 4: Ablation study of Skin-R1 across in-distribution and OOD datasets. **Bold** and underlined indicate the best and second-best performance, respectively.

Model	In-distribution						Avg.	Out-of-distribution (OOD)					Monk22	Avg.
	BCN20k	HAM10k	PAD	derm12345	derm7pt	dermnet		ISBI16	ISIC18	ISIC19	ISIC20			
Qwen2.5-VL-7B-Instruct	0.4911	0.5162	0.5033	0.3521	0.2962	0.4852	0.4367	0.3655	0.6301	0.6359	0.3325	<u>0.7078</u>	0.5027	
SFT	0.4899	0.6122	0.5358	0.4181	0.2937	0.4793	0.4743	0.5693	0.4509	0.5651	0.4249	<u>0.6039</u>	0.5153	
RL without SFT	0.5898	0.6671	0.5813	0.6056	0.3855	<u>0.5296</u>	0.5843	0.4223	0.7514	0.7208	0.3663	<b>0.7597</b>	0.5674	
Skin-R1 (500 steps)	<u>0.6139</u>	0.6870	0.6095	0.6020	0.3351	0.4882	0.5875	<u>0.6744</u>	0.6474	0.6805	<b>0.6848</b>	0.5519	0.6742	
Skin-R1 (1,000 steps)	0.6083	<u>0.7009</u>	<u>0.6508</u>	<u>0.6487</u>	<u>0.4502</u>	0.4956	<u>0.6156</u>	0.6660	0.7168	<b>0.7648</b>	0.5982	0.5909	<u>0.6870</u>	
Skin-R1 (1,500 steps)	<b>0.6345</b>	<b>0.7214</b>	<b>0.6573</b>	<b>0.6608</b>	<b>0.4955</b>	<b>0.5370</b>	<b>0.6385</b>	<b>0.6828</b>	<b>0.7630</b>	0.7630	0.6708	0.6494	<b>0.7171</b>	

Table 5: Ablation study of Skin-R1 on skin lesion diagnostic task across in-distribution datasets. **Bold** and underlined indicate the best and second-best performance, respectively.

Model	BCN20k				HAM10k				PAD				In-distribution				Avg.
	Acc	F1	Acc	F1	Acc	F1	Acc	F1	Derm12345	Derm7pt	DermNet	Acc	F1	Acc	F1		
Qwen2.5-VL-7B-Instruct	0.4308	0.3346	0.2905	0.2449	<u>0.4100</u>	<u>0.3632</u>	0.3046	0.2045	0.3661	0.3468	0.5399	0.4390	0.3698	0.2910			
SFT	0.4972	0.3228	0.6373	0.3567	0.3688	0.2970	0.8072	0.4037	0.6223	0.5876	0.6006	<u>0.4590</u>	0.6271	0.3868			
RL without SFT	0.4819	<b>0.3654</b>	0.3812	0.3037	<u>0.4338</u>	<b>0.3740</b>	0.4748	0.2839	0.3946	0.3824	0.5962	<b>0.4792</b>	0.4602	0.3414			
Skin-R1 (500 steps)	0.5229	0.3305	<b>0.7565</b>	0.3867	0.3362	0.2638	<u>0.8994</u>	0.4584	<b>0.7413</b>	0.6571	0.6036	0.4215	<b>0.6928</b>	0.4123			
Skin-R1 (1,000 steps)	0.5342	0.3528	0.6962	<u>0.3880</u>	0.3601	0.2916	0.8519	0.4421	0.6792	0.6386	<u>0.6228</u>	0.4325	0.6684	<u>0.4150</u>			
Skin-R1 (1,500 steps)	<b>0.5370</b>	0.3486	<u>0.7472</u>	<b>0.4039</b>	0.3536	0.2888	0.8918	<b>0.4786</b>	0.7089	<b>0.6589</b>	<u>0.6257</u>	0.4271	<b>0.6928</b>	<b>0.4287</b>			

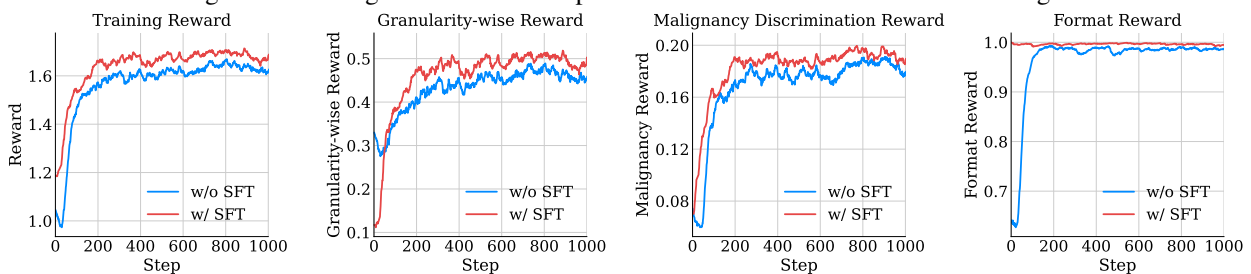
**Stage 1 (Trajectory SFT) Improves Diagnostic Ability and Structural Alignment.** SFT outperforms the **base model** Qwen2.5-VL-7B-Instruct overall. Furthermore, the **base model** suffers from formatting failures. When applying strict answer extraction, the **base model** fails to produce a valid answer in 30% of cases on the in-distribution diagnosis task as compared to SFT which fails in only 2% of the cases. We conclude that SFT plays a critically important role in achieving the substantial gains in both grounded diagnostic reasoning ability and structural alignment realized by Skin-R1.

**Stage 2 (RL) Significantly Boosts Performance and Generalization.** RL achieves markedly higher performance than all previous checkpoints and the **base model**. The reward design effectively drives the model to learn structured hierarchical reasoning and lesion differentiation through on-policy generation. Strong OOD results further validate its improved generalization. We choose the model at 1,000 step checkpoint as the representative model.

**High-Quality SFT is Essential for Effective RL.** The results show that the entire Skin-R1 pipeline comprehensively outperforms **RL without SFT**. Although **RL without SFT** improves on the **base model**, the best performance it achieves during training remains considerably lower (fig. 2). This suggests that an RL-only strategy, as applied in methods like Med-R1 [Lai et al., 2025] and MedVLM-R1 [Pan et al., 2025], provides limited enhancement due to lack of the grounded knowledge needed for robust reasoning. This comparison confirms that a high-quality SFT stage not only yields immediate performance gains but, more importantly, raises the model’s achievable performance for subsequent RL, resulting in stable performance gains and improved generalization.

We note that **RL without SFT** showed suboptimal performance at 1,000 steps, likely due to stochastic variation. Its best results occurred at 800 steps (0.5120 Accuracy, 0.3664 F1), and our conclusions remain consistent using this checkpoint.

Figure 2: Training reward curve comparison of Skin-R1 with or without SFT stage.



### 4.3 Targeted DDx and Hierarchical Evaluation

To evaluate DDx and hierarchy-aware reasoning, we introduce two targeted test sets: (1) *DDx diagnosis* and (2) *hierarchical diagnosis*. We adapt the standard in-distribution disease benchmark by systematically replacing distractors using the diagnostic taxonomy  $\mathcal{T}_{tax}$  and the differential diagnosis graph  $\mathcal{G}_{DDx}$  to increase task difficulty, respectively.

- For the hierarchical task, distractors are ancestor nodes (from  $\mathcal{T}_{tax}$ ) of the ground-truth. This tests the model’s ability to select the fine-grained diagnosis over its broader parent category.
- For the DDx task, distractors are confusable neighboring nodes (from  $\mathcal{G}_{DDx}$ ). This tests differentiation between clinically similar conditions.

As shown in fig. 3, Skin-R1 significantly achieves the highest accuracy in both settings. This demonstrates its superior robustness in differentiating visually similar diseases and its greater awareness of taxonomic relations. These results highlight the model’s enhanced ability to capture the fine-grained differential cues and structured knowledge required for dermatological reasoning.

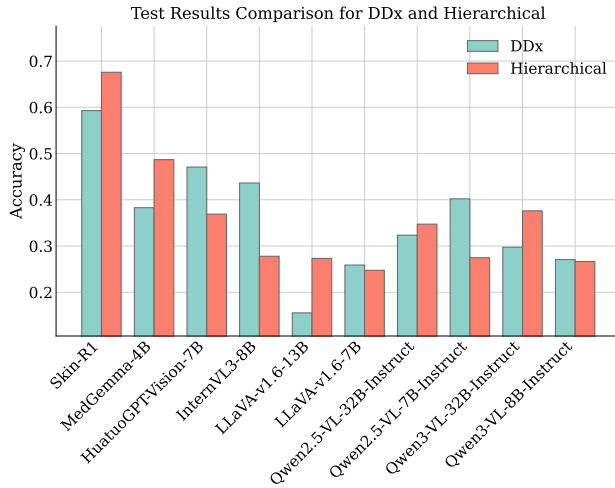


Figure 3: Comparison of Skin-R1 with baseline models on DDx and hierarchical diagnosis test sets.

### 4.4 Qualitative Analysis

Qualitative comparisons (see Appendix section E) confirm that Skin-R1 produces responses that are more concise, accurate, and consistent with expert diagnostic reasoning styles compared to the base Qwen2.5-VL-7B. This advantage stems from the grounded reasoning patterns instilled during trajectory SFT. This difference is clearly illustrated in Case 1 of Appendix section E. Skin-R1 demonstrates precise DDx reasoning, correctly concluding that features "...indicate a benign pigmented nevus rather than melanoma." This is a critical clinical distinction that the base Qwen2.5-VL-7B fails to capture.

The comparison highlights a key trade-off: while the base model provides more verbose descriptions, it suffers in diagnostic accuracy, the most critical aspect of clinical reasoning. Skin-R1, in contrast, achieves better precision and reliability, reflecting stronger grounded diagnostic reasoning capabilities.

## 5 Conclusion

In this paper, we have address three critical challenges that limit the trustworthiness and clinical utility of dermatological VLMs: dataset heterogeneity, the scarcity of grounded reasoning supervision, and the poor generalization of complex reasoning to large-scale, sparse-annotated datasets.

We introduced Skin-R1, a novel VLM trained via a systematic three-stage pipeline that combines deep, textbook-grounded supervision with the broad generalization capabilities of reinforcement learning to address these through a unified, end-to-end framework. First, we design a textbook-based reasoning generator that synthesizes high-fidelity, hierarchy-aware, and differential-diagnosis (DDx)-informed trajectories, providing reliable expert-level supervision. Second, we leverage the constructed trajectories for supervised fine-tuning (SFT) empowering the model with grounded

reasoning ability. Third, we develop a novel reinforcement learning (RL) paradigm that, by incorporating the hierarchical structure of diseases, effectively transfers these grounded reasoning patterns to large-scale, sparse data. Extensive experiments on multiple datasets demonstrate that Skin-R1 outperforms SOTA baselines on metrics that assess diagnostic accuracy and robustness. The ablation study demonstrates the importance of the reasoning foundation instilled by SFT.

## References

- Roderick J Hay, Nicole E Johns, Hywel C Williams, Ian W Bolliger, Robert P Dellavalle, David J Margolis, Robin Marks, Luigi Naldi, Martin A Weinstock, Sarah K Wulf, et al. The global burden of skin disease in 2010: an analysis of the prevalence and impact of skin conditions. *Journal of investigative dermatology*, 134(6):1527–1534, 2014.
- Hao Feng, Juliana Berk-Krauss, Paula W Feng, and Jennifer A Stein. Comparison of dermatologist density between urban and rural counties in the united states. *JAMA dermatology*, 154(11):1265–1271, 2018.
- Jack Resnick Jr and Alexa B Kimball. The dermatology workforce shortage. *Journal of the American Academy of Dermatology*, 50(1):50–54, 2004.
- Juxiao Zhou, Xiaonan He, Liyuan Sun, Jiannan Xu, Xiuying Chen, Yuetan Chu, Longxi Zhou, Xingyu Liao, Bin Zhang, Shawn Afvari, et al. Pre-trained multimodal large language model enhances dermatological diagnosis using skingpt-4. *Nature Communications*, 15(1):5649, 2024.
- Yuan Liu, Ayush Jain, Clara Eng, David H Way, Kang Lee, Peggy Bui, Kimberly Kanada, Guilherme de Oliveira Marinho, Jessica Gallegos, Sara Gabriele, et al. A deep learning system for differential diagnosis of skin diseases. *Nature medicine*, 26(6):900–908, 2020.
- Angel Alfonso Cruz-Roa, John Edison Arevalo Ovalle, Anant Madabhushi, and Fabio Augusto González Osorio. A deep learning architecture for image representation, visual interpretability and automated basal-cell carcinoma cancer detection. In *International conference on medical image computing and computer-assisted intervention*, pages 403–410. Springer, 2013.
- Yading Yuan, Ming Chao, and Yeh-Chi Lo. Automatic skin lesion segmentation using deep fully convolutional networks with jaccard distance. *IEEE transactions on medical imaging*, 36(9):1876–1886, 2017.
- Siyuan Yan, Xieji Li, Ming Hu, Yiwen Jiang, Zhen Yu, and Zongyuan Ge. Make: Multi-aspect knowledge-enhanced vision-language pretraining for zero-shot dermatological assessment. *arXiv preprint arXiv:2505.09372*, 2025a.
- Chanwoo Kim, Soham U Gadgil, Alex J DeGrave, Jesutofunmi A Omiye, Zhusu Ran Cai, Roxana Daneshjou, and Su-In Lee. Transparent medical image ai via an image–text foundation model grounded in medical literature. *Nature medicine*, 30(4):1154–1165, 2024.
- Siyuan Yan, Zhen Yu, Clare Primiero, Cristina Vico-Alonso, Zhonghua Wang, Litao Yang, Philipp Tschandl, Ming Hu, Lie Ju, Gin Tan, et al. A multimodal vision foundation model for clinical dermatology. *Nature Medicine*, pages 1–12, 2025b.
- Pang Wei Koh, Thao Nguyen, Yew Siang Tang, Stephen Mussmann, Emma Pierson, Been Kim, and Percy Liang. Concept bottleneck models. In *International conference on machine learning*, pages 5338–5348. PMLR, 2020.
- Siyuan Yan, Zhen Yu, Xuelin Zhang, Dwarikanath Mahapatra, Shekhar S Chandra, Monika Janda, Peter Soyer, and Zongyuan Ge. Towards trustable skin cancer diagnosis via rewriting model’s decision. In *Proceedings of the IEEE/CVF Conference on Computer Vision and Pattern Recognition*, pages 11568–11577, 2023.
- Lijie Hu, Songning Lai, Wenshuo Chen, Hongru Xiao, Hongbin Lin, Lu Yu, Jingfeng Zhang, and Di Wang. Towards multi-dimensional explanation alignment for medical classification. *Advances in Neural Information Processing Systems*, 37:129640–129671, 2024a.
- Roxana Daneshjou, Mert Yuksekgonul, Zhusu Ran Cai, Roberto Novoa, and James Y Zou. Skincon: A skin disease dataset densely annotated by domain experts for fine-grained debugging and analysis. *Advances in Neural Information Processing Systems*, 35:18157–18167, 2022.
- Dermnet. <https://www.kaggle.com/datasets/shubhamgoel27/dermnet>.
- Yuxiang Lai, Jike Zhong, Ming Li, Shitian Zhao, and Xiaofeng Yang. Med-r1: Reinforcement learning for generalizable medical reasoning in vision-language models. *arXiv preprint arXiv:2503.13939*, 2025.
- Jiazheng Pan, Che Liu, Junde Wu, Fenglin Liu, Jiayuan Zhu, Hongwei Bran Li, Chen Chen, Cheng Ouyang, and Daniel Rueckert. Medvilm-r1: Incentivizing medical reasoning capability of vision-language models (vlms) via reinforcement learning. In *International Conference on Medical Image Computing and Computer-Assisted Intervention*, pages 337–347. Springer, 2025.
- Shaohao Rui, Kaitao Chen, Weijie Ma, and Xiaosong Wang. Improving medical reasoning with curriculum-aware reinforcement learning. *arXiv preprint arXiv:2505.19213*, 2025.
- Tan-Hanh Pham and Chris Ngo. Rarl: Improving medical vlm reasoning and generalization with reinforcement learning and lora under data and hardware constraints. *arXiv preprint arXiv:2506.06600*, 2025.
- Wenhui Zhu, Xuanzhao Dong, Xin Li, Peijie Qiu, Xiwen Chen, Abolfazl Razi, Aris Sotiras, Yi Su, and Yalin Wang. Toward effective reinforcement learning fine-tuning for medical vqa in vision-language models. *arXiv preprint arXiv:2505.13973*, 2025a.

- Wenqi Zeng, Yuqi Sun, Chenxi Ma, Weimin Tan, and Bo Yan. Mm-skin: Enhancing dermatology vision-language model with an image-text dataset derived from textbooks. In *Proceedings of the 33rd ACM International Conference on Multimedia*, pages 3769–3778, 2025.
- Songtao Jiang, Yuan Wang, Sibo Song, Yan Zhang, Zijie Meng, Bohan Lei, Jian Wu, Jimeng Sun, and Zuozhu Liu. Omnipiv-med: Scaling medical vision-language model for universal visual understanding. *arXiv preprint arXiv:2504.14692*, 2025.
- Chunyuan Li, Cliff Wong, Sheng Zhang, Naoto Usuyama, Haotian Liu, Jianwei Yang, Tristan Naumann, Hoifung Poon, and Jianfeng Gao. Llava-med: Training a large language-and-vision assistant for biomedicine in one day. *Advances in Neural Information Processing Systems*, 36:28541–28564, 2023.
- Junying Chen, Chi Gui, Ruyi Ouyang, Anningzhe Gao, Shunian Chen, Guiming Hardy Chen, Xidong Wang, Ruifei Zhang, Zhenyang Cai, Ke Ji, et al. Huatuogpt-vision, towards injecting medical visual knowledge into multimodal llms at scale. *arXiv preprint arXiv:2406.19280*, 2024.
- Andrew Sellergren, Sahar Kazemzadeh, Tiam Jaroensri, Atilla Kiraly, Madeleine Traverse, Timo Kohlberger, Shawn Xu, Fayaz Jamil, Cian Hughes, Charles Lau, et al. Medgemma technical report. *arXiv preprint arXiv:2507.05201*, 2025.
- Shuai Bai, Keqin Chen, Xuejing Liu, Jialin Wang, Wenbin Ge, Sibo Song, Kai Dang, Peng Wang, Shijie Wang, Jun Tang, et al. Qwen2. 5-vl technical report. *arXiv preprint arXiv:2502.13923*, 2025.
- Haotian Liu, Chunyuan Li, Qingyang Wu, and Yong Jae Lee. Visual instruction tuning. *arXiv:2304.08485*, 2023.
- Deyao Zhu, Jun Chen, Xiaoqian Shen, Xiang Li, and Mohamed Elhoseiny. Minigpt-4: Enhancing vision-language understanding with advanced large language models. *arXiv preprint arXiv:2304.10592*, 2023.
- Shukang Yin, Chaoyou Fu, Sirui Zhao, Ke Li, Xing Sun, Tong Xu, and Enhong Chen. A survey on multimodal large language models. *arXiv preprint arXiv:2306.13549*, 2023.
- Muhammad Awais, Muzammal Naseer, Salman Khan, Rao Muhammad Anwer, Hisham Cholakkal, Mubarak Shah, Ming-Hsuan Yang, and Fahad Shahbaz Khan. Foundation models defining a new era in vision: a survey and outlook. *IEEE Transactions on Pattern Analysis and Machine Intelligence*, 2025.
- OpenAI. Gpt-4 technical report. 2023.
- Hugo Touvron, Thibaut Lavril, Gautier Izacard, Xavier Martinet, Marie-Anne Lachaux, Timothée Lacroix, Baptiste Rozière, Naman Goyal, Eric Hambro, Faisal Azhar, et al. Llama: Open and efficient foundation language models. *arXiv preprint arXiv:2302.13971*, 2023.
- Gemini Team, Rohan Anil, Sebastian Borgeaud, Yonghui Wu, Jean-Baptiste Alayrac, Jiahui Yu, Radu Soricut, Johan Schalkwyk, Andrew M Dai, Anja Hauth, et al. Gemini: a family of highly capable multimodal models. *arXiv preprint arXiv:2312.11805*, 2023.
- Weijieying Ren, Jingxi Zhu, Zehao Liu, Tianxiang Zhao, and Vasant Honavar. A comprehensive survey of electronic health record modeling: From deep learning approaches to large language models. *arXiv preprint arXiv:2507.12774*, 2025.
- Hongjian Zhou, Fenglin Liu, Boyang Gu, Xinyu Zou, Jinfang Huang, Jing Wu, Yiru Li, Sam S Chen, Peilin Zhou, Junling Liu, et al. A survey of large language models in medicine: Progress, application, and challenge. *arXiv preprint arXiv:2311.05112*, 2023.
- Dianzhe Tian, Shitao Jiang, Lei Zhang, Xin Lu, and Yiyao Xu. The role of large language models in medical image processing: a narrative review. *Quantitative Imaging in Medicine and Surgery*, 14(1):1108–1121, 2024.
- Zifeng Wang, Zhenbang Wu, Dinesh Agarwal, and Jimeng Sun. Medclip: Contrastive learning from unpaired medical images and text. In *Proceedings of the Conference on Empirical Methods in Natural Language Processing. Conference on Empirical Methods in Natural Language Processing*, volume 2022, page 3876, 2022.
- Ming Y Lu, Bowen Chen, Drew FK Williamson, Richard J Chen, Ivy Liang, Tong Ding, Guillaume Jaume, Igor Odintsov, Long Phi Le, Georg Gerber, et al. A visual-language foundation model for computational pathology. *Nature medicine*, 30(3):863–874, 2024.
- Omkar Thawkar, Abdelrahman Shaker, Sahal Shaji Mullappilly, Hisham Cholakkal, Rao Muhammad Anwer, Salman Khan, Jorma Laaksonen, and Fahad Shahbaz Khan. Xraygpt: Chest radiographs summarization using medical vision-language models. *arXiv preprint arXiv:2306.07971*, 2023.
- Yizhen Luo, Jiahuan Zhang, Siqi Fan, Kai Yang, Massimo Hong, Yushuai Wu, Mu Qiao, and Zaiqing Nie. Biomedgpt: An open multimodal large language model for biomedicine. *IEEE Journal of Biomedical and Health Informatics*, 2024.

- Tianwei Lin, Wenqiao Zhang, Sijing Li, Yuqian Yuan, Binhe Yu, Haoyuan Li, Wanggui He, Hao Jiang, Mengze Li, Xiaohui Song, et al. Healthgpt: A medical large vision-language model for unifying comprehension and generation via heterogeneous knowledge adaptation. *arXiv preprint arXiv:2502.09838*, 2025.
- Daya Guo, Dejian Yang, Haowei Zhang, Junxiao Song, Peiyi Wang, Qihao Zhu, Runxin Xu, Ruoyu Zhang, Shirong Ma, Xiao Bi, et al. Deepseek-r1 incentivizes reasoning in llms through reinforcement learning. *Nature*, 645(8081): 633–638, 2025.
- Tian Xie, Zitian Gao, Qingnan Ren, Haoming Luo, Yuqian Hong, Bryan Dai, Joey Zhou, Kai Qiu, Zhirong Wu, and Chong Luo. Logic-rl: Unleashing llm reasoning with rule-based reinforcement learning. *arXiv preprint arXiv:2502.14768*, 2025.
- Jiangjie Chen, Qianyu He, Siyu Yuan, Aili Chen, Zhicheng Cai, Weinan Dai, Hongli Yu, Qiying Yu, Xuefeng Li, Jiaze Chen, et al. Enigmata: Scaling logical reasoning in large language models with synthetic verifiable puzzles. *arXiv preprint arXiv:2505.19914*, 2025.
- Zhiyuan Hu, Yibo Wang, Hanze Dong, Yuhui Xu, Amrita Saha, Caiming Xiong, Bryan Hooi, and Junnan Li. Beyond'aha!': Toward systematic meta-abilities alignment in large reasoning models. *arXiv preprint arXiv:2505.10554*, 2025.
- Jingyi Zhang, Jiaxing Huang, Huanjin Yao, Shunyu Liu, Xikun Zhang, Shijian Lu, and Dacheng Tao. R1-vl: Learning to reason with multimodal large language models via step-wise group relative policy optimization. *arXiv preprint arXiv:2503.12937*, 2025.
- Tamera Lanham, Anna Chen, Ansh Radhakrishnan, Benoit Steiner, Carson Denison, Danny Hernandez, Dustin Li, Esin Durmus, Evan Hubinger, Jackson Kernion, et al. Measuring faithfulness in chain-of-thought reasoning. *arXiv preprint arXiv:2307.13702*, 2023.
- Jie Huang, Xinyun Chen, Swaroop Mishra, Huaixiu Steven Zheng, Adams Wei Yu, Xinying Song, and Denny Zhou. Large language models cannot self-correct reasoning yet. In *The Twelfth International Conference on Learning Representations*.
- Qwen Team. Qwq-32b: Embracing the power of reinforcement learning, March 2025. URL <https://qwenlm.github.io/blog/qwq-32b/>.
- Ilia Shumailov, Zakhar Shumaylov, Yiren Zhao, Nicolas Papernot, Ross Anderson, and Yarin Gal. Ai models collapse when trained on recursively generated data. *Nature*, 631(8022):755–759, 2024.
- Kun Wang, Guibin Zhang, Zhenhong Zhou, Jiahao Wu, Miao Yu, Shiqian Zhao, Chenlong Yin, Jinhu Fu, Yibo Yan, Hanjun Luo, et al. A comprehensive survey in llm (-agent) full stack safety: Data, training and deployment. *arXiv preprint arXiv:2504.15585*, 2025.
- Zhihong Shao, Peiyi Wang, Qihao Zhu, Runxin Xu, Junxiao Song, Xiao Bi, Haowei Zhang, Mingchuan Zhang, YK Li, Yang Wu, et al. Deepseekmath: Pushing the limits of mathematical reasoning in open language models. *arXiv preprint arXiv:2402.03300*, 2024.
- John Schulman, Filip Wolski, Prafulla Dhariwal, Alec Radford, and Oleg Klimov. Proximal policy optimization algorithms. *arXiv preprint arXiv:1707.06347*, 2017.
- Rafael Rafailov, Archit Sharma, Eric Mitchell, Christopher D Manning, Stefano Ermon, and Chelsea Finn. Direct preference optimization: Your language model is secretly a reward model. *Advances in neural information processing systems*, 36:53728–53741, 2023.
- Andre GC Pacheco and Renato A Krohling. The impact of patient clinical information on automated skin cancer detection. *Computers in biology and medicine*, 116:103545, 2020.
- Marc Combalia, Noel CF Codella, Veronica Rotemberg, Brian Helba, Veronica Vilaplana, Ofer Reiter, Cristina Carrera, Alicia Barreiro, Allan C Halpern, Susana Puig, et al. Bcn20000: Dermoscopic lesions in the wild. *arXiv preprint arXiv:1908.02288*, 2019.
- Abdurrahim Yilmaz, Sirlin Pekcan Yasar, Gulsum Gencoglan, and Burak Temelkuran. Derm12345: A large, multisource dermatoscopic skin lesion dataset with 40 subclasses. *Scientific Data*, 11(1):1302, 2024.
- Jeremy Kawahara, Sara Daneshvar, Giuseppe Argenziano, and Ghassan Hamarneh. Seven-point checklist and skin lesion classification using multitask multimodal neural nets. *IEEE Journal of Biomedical and Health Informatics*, 23(2):538–546, 2019. doi: 10.1109/JBHI.2018.2824327.
- Philipp Tschandl. The HAM10000 dataset, a large collection of multi-source dermatoscopic images of common pigmented skin lesions, 2018. URL <https://doi.org/10.7910/DVN/DBW86T>.

- Yutao Hu, Tianbin Li, Quanfeng Lu, Wenqi Shao, Junjun He, Yu Qiao, and Ping Luo. Omnimedvqa: A new large-scale comprehensive evaluation benchmark for medical lvm. In *Proceedings of the IEEE/CVF Conference on Computer Vision and Pattern Recognition*, pages 22170–22183, 2024b.
- Edward J Hu, Yelong Shen, Phillip Wallis, Zeyuan Allen-Zhu, Yuanzhi Li, Shean Wang, Lu Wang, and Weizhu Chen. LoRA: Low-rank adaptation of large language models. In *International Conference on Learning Representations*, 2022. URL <https://openreview.net/forum?id=nZeVKeeFYf9>.
- Qwen AI / Alibaba Cloud. Qwen3-vl: Sharper vision, deeper thought, broader action. Blog post, Oct 2025. URL <https://qwen.ai/blog?id=99f0335c4ad9ff6153e517418d48535ab6d8afef&from=research.latest-advancements-list>. Accessed: 2025-11-04.
- Jinguo Zhu, Weiyun Wang, Zhe Chen, Zhaoyang Liu, Shenglong Ye, Lixin Gu, Hao Tian, Yuchen Duan, Weijie Su, Jie Shao, et al. Internvl3: Exploring advanced training and test-time recipes for open-source multimodal models. *arXiv preprint arXiv:2504.10479*, 2025b.
- Haotian Liu, Chunyuan Li, Yuheng Li, Bo Li, Yuanhan Zhang, Sheng Shen, and Yong Jae Lee. Llavanext: Improved reasoning, ocr, and world knowledge, 2024.
- Matthew Groh, Caleb Harris, Luis Soenksen, Felix Lau, Rachel Han, Aerin Kim, Arash Koochek, and Omar Badri. Evaluating deep neural networks trained on clinical images in dermatology with the fitzpatrick 17k dataset. In *Proceedings of the IEEE/CVF Conference on Computer Vision and Pattern Recognition*, pages 1820–1828, 2021.
- Noel CF Codella, David Gutman, M Emre Celebi, Brian Helba, Michael A Marchetti, Stephen W Dusza, Aadi Kalloo, Konstantinos Liopyris, Nabin Mishra, Harald Kittler, et al. Skin lesion analysis toward melanoma detection: A challenge at the 2017 international symposium on biomedical imaging (isbi), hosted by the international skin imaging collaboration (isic). In *2018 IEEE 15th international symposium on biomedical imaging (ISBI 2018)*, pages 168–172. IEEE, 2018.
- Noel Codella, Veronica Rotemberg, Philipp Tschandl, M Emre Celebi, Stephen Dusza, David Gutman, Brian Helba, Aadi Kalloo, Konstantinos Liopyris, Michael Marchetti, et al. Skin lesion analysis toward melanoma detection 2018: A challenge hosted by the international skin imaging collaboration (isic). *arXiv preprint arXiv:1902.03368*, 2019.
- Skin lesion classification via the international skin imaging collaboration (isic) 2019 challenge. <https://challenge.isic-archive.com/landing/2019/>, 2019.
- Veronica Rotemberg, Nicholas Kurtansky, Brigid Betz-Stablein, Liam Caffery, Emmanouil Chousakos, Noel Codella, Marc Combalia, Stephen Dusza, Pascale Guitera, David Gutman, et al. A patient-centric dataset of images and metadata for identifying melanomas using clinical context. *Scientific data*, 8(1):34, 2021.
- Towhidul Islam, Mohammad Arafat Hussain, Forhad Uddin Hasan Chowdhury, and BM Riazul Islam. A web-scraped skin image database of monkeypox, chickenpox, smallpox, cowpox, and measles. *biorxiv*, pages 2022–08, 2022.
- Leandro von Werra, Younes Belkada, Lewis Tunstall, Edward Beeching, Tristan Thrush, Nathan Lambert, Shengyi Huang, Kashif Rasul, and Quentin Gallouédec. Trl: Transformer reinforcement learning. <https://github.com/huggingface/trl>, 2020.
- Hugging Face. Open r1: A fully open reproduction of deepseek-r1, January 2025. URL <https://github.com/huggingface/open-r1>.

## A Details of Datasets

We apply six datasets for the reinforcement learning training, PAD-UFES-20 [Pacheco and Krohling, 2020], DermNet [der], BCN20000 [Combalia et al., 2019], DERM12345[Yilmaz et al., 2024], Derm7pt[Kawahara et al., 2019], HAM10000[Tschandl, 2018].

Table 6: Summary of Datasets

Dataset	# images	# Disease
PAD-UFES-20 [Pacheco and Krohling, 2020]	2298	6
DermNet [der]	19500	23/600+
BCN20000 [Combalia et al., 2019]	18946	8
DERM12345 [Yilmaz et al., 2024]	12345	5/15/40
Derm7pt [Kawahara et al., 2019]	1011	5/20
HAM10000 [Tschandl, 2018]	10015	7

**PAD-UFES-20** [Pacheco and Krohling, 2020] PAD-UFES-20 is a dermoscopic and clinical skin image data set collected by the Federal University of Espírito Santo (UFES), Brazil. It contains 2,298 images of six types of lesion obtained from mobile devices in real clinical settings. In addition to image data, it provides 22 clinical and demographic features (e.g., age, sex, anatomical site).

**DermNet** [der] DermNet is a large-scale clinical dermatology image collection that contains approximately 19,500 images spanning 23 coarse- and more than 600 fine-grained disease categories. Each image is annotated with rich meta-features (23 total). To reduce data noise and improve training efficiency, we preprocessed DermNet by filtering out approximately 80% of the samples. Specifically, we excluded a large number of rare diseases from the long-tailed distribution and retained only those categories relevant to skin cancers and their differential diagnoses, which align with the scope of this study.

**BCN20000** [Combalia et al., 2019] BCN20000 was introduced by the Hospital Clínic de Barcelona as a curated dermoscopic image data set that contains 18,946 images from 8 diagnostic classes. The data set includes clinical metadata such as patient age, sex, and location of the lesion. It serves as a high-quality benchmark for training models in automated skin lesion classification and melanoma detection.

**DERM12345** [Yilmaz et al., 2024] DERM12345 is a hierarchical dermatology dataset consisting of 12,345 dermoscopic and clinical images which introduces multi-granular lesion categorization across three taxonomy levels (5 / 15 / 40 classes), providing structured hierarchical labels rather than single flat categories. The data set emphasizes hierarchical reasoning for fine-grained dermatological diagnosis.

**Derm7pt** [Kawahara et al., 2019] Derm7pt is a publicly available dermoscopic dataset containing 1,011 images annotated according to the 7-point melanoma checklist criteria. It includes seven clinical features (e.g., atypical network, blue-white veil, streaks, regression structures) and lesion labels for 20 diagnostic categories.

**HAM10000** [Tschandl, 2018] HAM10000 (“Human Against Machine with 10,000 Training Images”) is one of the most widely used dermoscopic datasets, containing 10,015 images from 7 diagnostic categories collected from multiple sources which provides a balanced representation of benign and malignant lesions, including melanoma, melanocytic nevus, basal cell carcinoma, actinic keratosis, benign keratosis, dermatofibroma, and vascular lesions.

Each of the six datasets is divided into training, validation and test subsets following either their official splits or, when such information is unavailable, a random split with a ratio of 6:2:2. Note that the validation set is not used in our training or evaluation processes. It is retained primarily to maintain compatibility with the data sets that originally provided a three-way split. The total size of the training set is 26,507, and the test set contains 8,390 samples.

**Multiple-option form method of in-distribution dataset.** To construct reasonable multiple-choice options consistent with the principle of hierarchical taxonomy, the options for each instance are randomly sampled from both the taxonomy tree of its corresponding dataset and the shared global taxonomy tree.

For RL training, the granularity-wise reward  $R_{gran}$  is assigned following the procedure described in the **Granularity-wise Reward** subsection of section 3.2.2. Specifically, the granularity-wise reward value of each option corresponds to its level within the general taxonomy tree if it is on the correct taxonomy path and is set to 0 if it is on an incorrect path.

For evaluation of disease diagnosis, only the most fine-grained option located on the correct taxonomy path among all candidates is considered the correct answer. For evaluation of diagnosis of lesion conditions, the same instances of the testing set are applied and the corresponding options are replaced as A: **benign**, B: **malignant**, C: **precancerous in situ**. The applied prompt templates are given in the Appendix section D.

**Dataset of out-of-distribution (OOD) disease diagnosis task.** In addition to the test subsets of the six datasets above, we further evaluate the generalizability of the proposed model using the OmniMedVQA dermoscopy subset [Hu et al., 2024b]. OmniMedVQA is a large-scale comprehensive medical visual question-answering (VQA) benchmark. It draws from 73 publicly-available medical datasets, spans 12 imaging modalities (e.g., dermoscopy, MRI, CT, X-ray, histopathology). In total, it includes 118,010 real clinical images and 127,995 QA items, converted into a multi-choice VQA format with incorrect options appended for each question.

This subset integrates multiple public datasets, including Fitzpatrick17k[Groh et al., 2021] (excluded), ISBI2016 [Codella et al., 2018], ISIC2018 [Codella et al., 2019], ISIC2019 [ISI, 2019], ISIC2020 [Rotemberg et al., 2021], Monkeypox Skin Image 2022 [Islam et al., 2022] and PAD-UFES-20 [Pacheco and Krohling, 2020] (excluded). The detailed statics of the OmniMedVQA dermoscopy subset is shown in table 7. To accurately reflect the diagnostic capability of our model, we use only the samples with "question\_type": "Disease Diagnosis", while those labeled as "Modality Recognition" and "Anatomy Identification" are excluded from the evaluation. Furthermore, since Fitzpatrick 17k, which is one of the original datasets included in the SkinCon collection [Daneshjou et al., 2022] and used for the concept alignment training of Skin-R1, and PAD-UFES-20, which is utilized during the RL training stage, overlap with samples in OmniMedVQA, the corresponding subsets are excluded from the OmniMedVQA evaluation to avoid data duplication.

Table 7: Dataset distribution

Dataset	Count	Percentage
Fitzpatrick 17k (excluded)	1,287	24.16%
ISBI2016	476	8.94%
ISIC2018	173	3.25%
ISIC2019	1,637	30.74%
ISIC2020	1,212	22.76%
Monkeypox Skin Image 2022	154	2.89%
PAD-UFES-20 (excluded)	387	7.27%
<b>Total</b>	<b>5,326</b>	<b>100.00%</b>

## B Details of Trajectory Construction

In this section, the construction details of 3 types of trajectory dataset  $\mathcal{S}_1, \mathcal{S}_2, \mathcal{S}_3$  are provided.

**Synthesis of Type 1 Trajectories.** To generate Type 1 diagnostic trajectories, we synthesize direct image-to-diagnosis mappings based on the curated diagnostic case set  $\mathcal{D}_{case} = \{(I_i, r_i, d_i)\}_{i=1}^N$ , where  $I_i$  denotes the clinical image,  $r_i$  the corresponding diagnostic rationale, and  $d_i$  the confirmed diagnosis. As summarized in algorithm 1, the procedure iterates over each record  $(I_i, r_i, d_i) \in \mathcal{D}_{case}$ . For each case, we retrieve the associated taxonomic information  $t_f$ , which includes the hierarchical path of  $d_i$  in  $\mathcal{T}_{tax}$ , i.e.,  $path_{\mathcal{T}_{tax}}(d_i)$  and its malignancy indicator  $malig(d_i) \in \{benign, malignant, precancerous in situ\}$ . A Type 1 trajectory instance is then constructed as

$\tau^{(1)} \leftarrow (I_i, r_i, d_i, t_f)$  representing a direct, single-step reasoning trace from the visual input to the final diagnosis.

---

### Algorithm 1 Synthesis of Type 1 Trajectories

---

**Input:** Dataset  $\mathcal{D}_{case} = \{(I_i, r_i, d_i)\}_{i=1}^N$ , taxonomy  $\mathcal{T}_{tax}$

**Output:** Set of trajectories  $\mathcal{S}_1$

- 1:  $\mathcal{S}_1 \leftarrow \emptyset$
  - 2: **for**  $(I_i, r_i, d_i) \in \mathcal{D}_{case}$  **do**
  - 3:    $t_f \leftarrow (path_{\mathcal{T}_{tax}}(d_i), malig(d_i))$
  - 4:    $\tau^{(1)} \leftarrow (I_i, r_i, d_i, t_f)$
  - 5:    $\mathcal{S}_1 \leftarrow \mathcal{S}_1 \cup \{\tau^{(1)}\}$
  - 6: **end for**
  - 7: **return**  $\mathcal{S}_1$
-

Table 8: Summary of key notations

Symbol	Description
<i>1. Base Data Units</i>	
$I$	Clinical image.
$\mathcal{C}$	Set of associated concept terms for an image.
$c_j$	Specific concept term from $\mathcal{C}$ .
$d, d_i$	Diagnosis.
$r, r_i$	Textual rationale associated with a diagnostic case.
$p_i$	Instructional prompt used for generation tasks.
$e_i$	Detailed concept explanation generated by an LLM.
$t$	Hierarchical taxonomic annotation of a disease.
<i>2. Datasets &amp; Knowledge Bases</i>	
$\mathcal{D}_{\text{source}}$	Original source dataset (SkinCon).
$\mathcal{D}_{\text{pairs}}$	Dataset of decomposed (image, concept) pairs.
$\mathcal{D}_{\text{concept}}$	Fine-grained concept explanation dataset.
$\mathcal{D}_{\text{cases}}$	Diagnostic cases extracted from textbooks.
$\mathcal{D}_{\text{traj}}$	Constructed diagnostic trajectory dataset.
$\mathcal{T}$	Hierarchical diagnostic taxonomy.
$\mathcal{D}\mathcal{X}$	Differential diagnosis (DDX) graph.
<i>3. Diagnostic Trajectory Components</i>	
$\tau^{(1)}, \tau^{(2)}, \tau^{(3)}$	Three trajectory types (Type 1, 2, 3).
$d_p, r_p$	Primary diagnosis and rationale.
$d_d, r_d$	Differential diagnosis and rationale.
$\rho$	Differential reasoning process.
$d_f, t_f$	Final diagnosis and its taxonomy.
<i>4. Functions &amp; Indices</i>	
$f_{\text{LLM}}$	LLM function for generating explanations.
$N, M$	Number of samples or instances.

**Synthesis of Type 2 Trajectories.** Type 2 trajectories introduce differential diagnosis (DDX) reasoning while retaining the correct primary diagnosis. As described in algorithm 2, for each diagnostic case  $(I_i, r_p, d_p) \in \mathcal{D}$ , the algorithm first retrieves a clinically related differential diagnosis  $d_d$  by querying the differential diagnosis graph  $\mathcal{G}_{DDx}$  and the taxonomy  $\mathcal{T}_{tax}$  through the RESOLVEDDXNEIGHBOR function. If there is no valid neighbor, a random alternative disease is sampled from  $\mathcal{D} \setminus \{d_p\}$  to ensure diversity and maintain balanced differential supervision. For a selected differential case  $(I_j, r_d, d_d)$ , an LLM comparator generates the explicit differential reasoning statement  $\rho = \text{LLM}(r_p, r_d, d_p)$ , which highlights the discriminative features that distinguish  $d_p$  from  $d_d$ . Since this trajectory represents a non-revision scenario, the final diagnosis remains unchanged ( $d_f = d_p$ ), and its corresponding taxonomic information is denoted as  $t_f = (\text{path}_{\mathcal{T}_{tax}}(d_f), \text{malig}(d_f))$ . Thus, a complete Type 2 trajectory instance is constructed as

$$\tau^{(2)} = (I_i, r_p, d_p, r_d, d_d, \rho, d_f, t_f),$$

and appended to the set of trajectories  $\mathcal{S}_2$ . This process yields a collection of contrastive yet stable diagnostic examples in which differential reasoning is explicitly modeled but the final decision remains consistent with the primary diagnosis, thereby teaching the model to resist misleading differentials while maintaining diagnostic confidence.

**Algorithm 2** Synthesis of Type 2 Trajectories (No Revision)

---

**Input:** Dataset  $\mathcal{D} = \{(I_i, r_i, d_i)\}_{i=1}^N$ , taxonomy  $\mathcal{T}_{tax}$ , DDX graph  $\mathcal{G}_{DDx}$ , LLM comparator  
**Output:** Set  $\mathcal{S}_2$

- 1:  $\mathcal{S}_2 \leftarrow \emptyset$
- 2: **for**  $(I_i, r_p, d_p) \in \mathcal{D}$  **do**
- 3:    $d_d \leftarrow \text{RESOLVEDDXNEIGHBOR}(d_p, \mathcal{G}_{DDx}, \mathcal{T}_{tax}, \mathcal{D}_{case})$
- 4:   **if**  $d_d = \text{NONE}$  **then**
- 5:      $d_d \leftarrow \text{RANDOMSAMPLE}(\mathcal{D}_{case} \setminus \{d_p\})$
- 6:   **end if**
- 7:   select  $(I_j, r_d, d_d) \in \mathcal{D}_{case}$  with  $d_d$
- 8:    $\rho \leftarrow \text{LLM}(r_p, r_d, d_p)$
- 9:    $d_f \leftarrow d_p$ ;  $t_f \leftarrow (\text{path}_{\mathcal{T}_{tax}}(d_f), \text{malig}(d_f))$
- 10:    $\tau^{(2)} \leftarrow (I_i, r_p, d_p, r_d, d_d, \rho, d_f, t_f)$
- 11:    $\mathcal{S}_2 \leftarrow \mathcal{S}_2 \cup \{\tau^{(2)}\}$
- 12: **end for**
- 13: **return**  $\mathcal{S}_2$

---

**Synthesis of Type 3 Trajectories.** Type 3 trajectories extend the differential diagnosis (DDX) reasoning introduced in Type 2 by modeling *reflective revision*, in which the model corrects an initially incorrect primary diagnosis after differential comparison. As shown in algorithm 3, the overall procedure follows the same data retrieval and pairing process as in Type 2: for each diagnostic case  $(I_i, r_p, d_p) \in \mathcal{D}_{case}$ , a differential counterpart  $d_d$  is first identified using the RESOLVEDDXNEIGHBOR function over the DDX graph  $\mathcal{G}_{DDx}$  and taxonomy  $\mathcal{T}_{tax}$ . If no suitable neighbor exists, a random disease is sampled from  $\mathcal{D}_{case} \setminus \{d_p\}$  to ensure diversity. The paired differential case  $(I_j, r_d, d_d)$  is then used to generate an explicit reasoning statement  $\rho = \text{LLM}(r_p, r_d, d_d)$ , emphasizing the reflective process that justifies the correction. In this scenario, the final diagnosis is revised to the differential one ( $d_f = d_d$ ), and its taxonomic information is denoted as  $t_f = (\text{path}_{\mathcal{T}_{tax}}(d_f), \text{malig}(d_f))$ . A Type 3 trajectory instance is thus represented as

$$\tau^{(3)} = (I_i, r_p, d_p, r_d, d_d, \rho, d_f, t_f),$$

and collected into the trajectory set  $\mathcal{S}_3$ . Compared with Type 2 trajectories, which encode stable reasoning without revision, Type 3 trajectories explicitly capture the corrective dynamics of clinical reasoning, enabling the model to internalize reflective judgment and improve robustness when confronting ambiguous or misleading visual cues.

**Algorithm 3** Synthesis of Type 3 Trajectories (Reflective Revision)

---

**Input:** Dataset  $\mathcal{D}_{case} = \{(I_i, r_i, d_i)\}_{i=1}^N$ , taxonomy  $\mathcal{T}_{tax}$ , DDX graph  $\mathcal{G}_{DDx}$ , LLM comparator  
**Output:** Set  $\mathcal{S}_3$

- 1:  $\mathcal{S}_3 \leftarrow \emptyset$
- 2: **for**  $(I_i, r_p, d_p) \in \mathcal{D}_{case}$  **do**
- 3:    $d_d \leftarrow \text{RESOLVEDDXNEIGHBOR}(d_p, \mathcal{G}_{DDx}, \mathcal{T}_{tax}, \mathcal{D}_{case})$
- 4:   **if**  $d_d = \text{NONE}$  **then**
- 5:      $d_d \leftarrow \text{RANDOMSAMPLE}(\mathcal{D}_{case} \setminus \{d_p\})$
- 6:   **end if**
- 7:   select  $(I_j, r_d, d_d) \in \mathcal{D}_{case}$  with  $d_d$
- 8:    $\rho \leftarrow \text{LLM}(r_p, r_d, d_d)$
- 9:    $d_f \leftarrow d_d$ ;  $t_f \leftarrow (\text{path}_{\mathcal{T}_{tax}}(d_f), \text{malig}(d_f))$
- 10:    $\tau^{(3)} \leftarrow (I_i, r_p, d_p, r_d, d_d, \rho, d_f, t_f)$
- 11:    $\mathcal{S}_3 \leftarrow \mathcal{S}_3 \cup \{\tau^{(3)}\}$
- 12: **end for**
- 13: **return**  $\mathcal{S}_3$

---

**Differential Diagnosis (DDX) Fallback Policy.** To ensure reliable differential pairing even when direct graph connections are missing, we design a hierarchical DDX fallback policy, implemented in algorithm 4. Given a diagnosis node  $d$ , the algorithm first queries its neighborhood in the differential diagnosis graph  $\mathcal{G}_{DDx}$ . If  $d$  is not present in  $\mathcal{G}_{DDx}$  or lacks adjacent nodes, its taxonomy parent in  $\mathcal{T}_{tax}$  is queried as a higher-level surrogate. Once a set of candidate neighbors  $\mathcal{C}$  is obtained, the algorithm searches for a diagnosis  $c \in \mathcal{C}$  that has at least one associated case  $(I_k, r_k, d_k)$  in the dataset  $\mathcal{D}_{case}$ . If such a case does not exist, the algorithm recursively examines the taxonomy children of  $c$  to locate

a subclass  $c'$  with available samples. If neither direct neighbors nor fallback subclasses yield a match, the function returns **NONE**.

This hierarchical fallback mechanism guarantees that most differential pairs can be grounded in clinically related disease entities while preserving semantic consistency across the taxonomy and DDX graph. Balances It balances coverage and precision—providing robust DDX retrieval even for underrepresented conditions—thereby preventing the sparse nodes in  $\mathcal{G}_{DDx}$  from hindering the construction of reasoning-aware trajectories.

---

**Algorithm 4** ResolveDDXNeighbor: Find a DDX neighbor diagnosis with taxonomy fallbacks

---

**Input:** Diagnosis  $d$ , DDX graph  $\mathcal{G}_{DDx}$ , taxonomy  $\mathcal{T}_{tax}$ , dataset  $\mathcal{D}_{case}$

**Output:** A neighbor diagnosis  $\tilde{d}$  or **NONE**

```

1:  $\mathcal{C} \leftarrow \emptyset$ 
2: if  $d \in \mathcal{V}(\mathcal{G}_{DDx})$  and  $\text{Adj}_{\mathcal{G}_{DDx}}(d) \neq \emptyset$  then
3:    $\mathcal{C} \leftarrow \text{Adj}_{\mathcal{G}_{DDx}}(d)$ 
4: else
5:    $p \leftarrow \text{parent}_{\mathcal{T}_{tax}}(d)$ 
6:   if  $p \in \mathcal{V}(\mathcal{G}_{DDx})$  and  $\text{Adj}_{\mathcal{G}_{DDx}}(p) \neq \emptyset$  then
7:      $\mathcal{C} \leftarrow \text{Adj}_{\mathcal{G}_{DDx}}(p)$ 
8:   else
9:     return NONE
10:  end if
11: end if
12: for all  $c \in \mathcal{C}$  do
13:   if exists  $(I_k, r_k, d_k) \in \mathcal{D}_{case}$  with  $d_k = c$  then
14:     return  $c$ 
15:   else
16:      $\mathcal{S} \leftarrow \text{children}_{\mathcal{T}_{tax}}(c)$ 
17:     if exists  $(I_k, r_k, d_k) \in \mathcal{D}_{case}$  with  $d_k \in \mathcal{S}$  then
18:       return any  $c' \in \mathcal{S}$ 
19:     end if
20:   end if
21: end for
22: return NONE

```

---

**An example of the type 1 trajectory**



**Prompt:** You are a medical vision-language assistant specializing in dermatology. Given the dermatology image, analyze the visual findings and provide a structured diagnosis following this format:

<thinking>Describe the key clinical features, visual observations, and the diagnostic rationale that support the diagnosis.</thinking> <diagnosis>Provide the most likely and specific fine-grained diagnosis, and briefly classify the condition (benign or malignant) along with any relevant clinical taxonomy.</diagnosis>

Ensure your response is medically accurate, concise, and strictly follows the specified format.

---

**Response:** <thinking>Presence of a rough surface and stuck-on appearance indicates seborrheic keratosis.</thinking>

<diagnosis>seborrheic keratosis, Seborrheic keratosis is a subtype of benign keratosis-like lesion, and is generally classified as benign.</diagnosis>

## An example of the type 2 trajectory



**Prompt:** You are a medical vision-language assistant specializing in dermatology. Given the dermatology image, analyze the visual findings and provide a structured diagnostic reasoning following this format:

<thinking> Begin by describing the characteristic clinical features and visual observations of the lesion. Based on these features, propose the most likely diagnosis. Then, identify at least one plausible alternative diagnosis and describe its defining features. Compare the observed lesion with these alternatives, and explain step by step why the final diagnosis is more consistent with the findings. Conclude the reasoning with the single condition that best matches the clinical presentation. </thinking>

<diagnosis> Provide only the single most likely and specific fine-grained diagnosis. Also briefly classify the condition (benign or malignant) and indicate any relevant clinical taxonomy (e.g., subtype or disease family). Do not include explanations, multiple options, or extra punctuation. </diagnosis>

Ensure your response is medically accurate, concise, and strictly follows the specified format.

---

**Response:** <thinking>

Based on the rule: Presence of an erythematous, scaly, thin plaque around the cuticular margin or a verrucous plaque in the periungual region with nail discoloration, onycholysis, or destruction of the nail plate indicates Bowen disease of the nail unit. We can give a primary diagnosis that bowen disease of the nail unit. Considering the differential diagnosis for bowen disease of the nail unit, namely actinic keratosis, we compare against the diagnostic rule for actinic keratosis: Presence of hypertrophic actinic keratoses on severely sun-damaged dorsal arm skin with histopathology showing atypical basal and suprabasal keratinocytes, hyperchromatic and pleomorphic nuclei, partial loss of basal layer architecture without full-thickness epidermal involvement, alternating hyperorthokeratosis and hyperparakeratosis ("flag sign"), and underlying solar elastosis indicates actinic keratosis.

The lesion presents as an erythematous, scaly, thin plaque localized around the cuticular margin with nail discoloration and onycholysis, which aligns with Bowen disease of the nail unit. In contrast, the features typical of actinic keratosis, such as hypertrophic lesions on severely sun-damaged dorsal arm skin and the presence of alternating hyperorthokeratosis and hyperparakeratosis ("flag sign"), are absent. Additionally, the lesion is periungual rather than on sun-exposed dorsal skin, and there is no mention of the Therefore, the most likely condition corresponds to "bowen disease of the nail unit".

</thinking>

<diagnosis>bowen disease of the nail unit. Bowen disease of the nail unit is a subtype of bowen disease, and squamous cell carcinoma, and is generally classified as malignant.</diagnosis>

## An example of the type 3 trajectory



**Prompt:** You are a medical vision-language assistant specializing in dermatology. Given the dermatology image, analyze the visual findings and provide a structured diagnostic reasoning following this format:

<thinking> Begin by describing the characteristic clinical features and visual observations of the lesion. Based on these features, propose the most likely diagnosis. Then, identify at least one plausible alternative diagnosis and describe its defining features. Compare the observed lesion with these alternatives, and explain step by step why the final diagnosis is more consistent with the findings. Conclude the reasoning with the single condition that best matches the clinical presentation. </thinking>

<diagnosis> Provide only the single most likely and specific fine-grained diagnosis. Also briefly classify the condition (benign or malignant) and indicate any relevant clinical taxonomy (e.g., subtype or disease family). Do not include explanations, multiple options, or extra punctuation. </diagnosis>

Ensure your response is medically accurate, concise, and strictly follows the specified format.

**Response:** Based on the rule: Presence of multiple pigmented patches or thin papules with a reticulated pattern indicates reticulated seborrheic keratoses. We can give a primary diagnosis that reticulated seborrheic keratosis. Considering the differential diagnosis for reticulated seborrheic keratosis, namely melanoma, we compare against the diagnostic rule for melanoma: Presence of nests of melanocytes in the lower epidermis and dermis that vary in size and shape, become confluent, and lack maturation with descent into the dermis, combined with predominance of single melanocytes over nests and aberrant distribution, indicates melanoma.

The lesion exhibits irregularly distributed pigmented areas with variable size and shape, consistent with the presence of atypical melanocytes as described in melanoma. The absence of a uniform reticulated pattern and lack of multiple thin papules argue against reticulated seborrheic keratosis. Additionally, the predominance of single melanocytes rather than well-formed nests supports melanoma over seborrheic keratosis. Therefore, the most likely condition corresponds to "melanoma".

</thinking>

<diagnosis>melanoma. Melanoma is generally classified as malignant.</diagnosis>

## C Implementation Details

Training is performed using two NVIDIA A100 GPUs (40 GB VRAM each). We adopt Qwen2.5-VL-7B-Instruct [Bai et al., 2025] as the backbone model. Both SFT and RL stages are trained with the LoRA technique [Hu et al., 2022], using the following hyperparameters: `lora_r=64`, `lora_alpha=32`, and `lora_dropout=0.1`.

The SFT experiments are implemented using the TRL framework [von Werra et al., 2020]. Training is conducted with a total batch size of 16 and a learning rate of  $3 \times 10^{-5}$  for 4 epochs.

RL experiments are implemented and modified on the basis of the OpenR1 framework [Hugging Face, 2025]. Training is carried out with a total batch size of 16 and a learning rate of  $1 \times 10^{-5}$  for 1 epoch. The group size  $K$  in GRPO is set to 4, and the sampling temperature is fixed at 1.0. The reference model is initialized from the SFT checkpoint. The maximum input image resolution is capped at  $448 \times 448 = 200,704$  pixels.

During the evaluation, to guarantee the certainty of the result, greedy decoding is applied, which means that all the models are set as `do_sample = False`. The maximum input image resolution is also set to  $448 \times 448 = 200,704$  pixels.

**Details of Baselines.** LLaVA-v1.6-7B [Liu et al., 2024] corresponds to the Hugging Face release *liuhaotian/llava-v1.6-mistral-7b*. LLaVA-Med-7B [Li et al., 2023] corresponds to *microsoft/llava-med-v1.5-mistral-7b*, and HuatuoGPT-Vision-7B [Chen et al., 2024] corresponds to *FreedomIntelligence/HuatuoGPT-Vision-7B-Qwen2.5VL*. In particular, due to their limited CoT reasoning and instruction-following capabilities, the prompts for LLaVA-Med-7B and SkinVL-PubMM are simplified to ensure meaningful response generation. Detailed prompt templates are provided in Appendix section D.

## D Details of Prompts

### Prompt template for SFT, type 1

You are a medical vision-language assistant specializing in dermatology. Given the dermatology image, analyze the visual findings and provide a structured diagnosis following this format:

<thinking>Describe the key clinical features, visual observations, and the diagnostic rationale that support the diagnosis.</thinking> <diagnosis>Provide the most likely and specific fine-grained diagnosis, and briefly classify the condition (benign or malignant) along with any relevant clinical taxonomy.</diagnosis>

Ensure your response is medically accurate, concise, and strictly follows the specified format.

### Prompt template for SFT, type 2 and 3

You are a medical vision-language assistant specializing in dermatology. Given the dermatology image, analyze the visual findings and provide a structured diagnostic reasoning following this format:

<thinking> Begin by describing the characteristic clinical features and visual observations of the lesion. Based on these features, propose the most likely diagnosis. Then identify at least one plausible alternative diagnosis and describe its defining features. Compare the observed lesion with these alternatives and explain step by step why the final diagnosis is more consistent with the findings. Conclude the reasoning with the single condition that best matches the clinical presentation. </thinking>

<diagnosis> Provide only the single most likely and specific fine-grained diagnosis. Also briefly classify the condition (benign or malignant) and indicate any relevant clinical taxonomy (e.g., subtype or disease family). Do not include explanations, multiple options, or extra punctuation. </diagnosis>

Ensure your response is medically accurate, concise, and strictly follows the specified format.

### Prompt template for RL training

**Question example** = What type of abnormality is present in this image? A: actinic keratosis B: melanoma C: benign keratosis-like lesion D: squamous cell carcinoma

You are a medical vision-language assistant specializing in dermatology. Given the dermatology image, answer:

#### Question example

Provide necessary reasoning and only answer the question in the following format:

<thinking>Describe the key clinical features and visual observations that support your diagnosis.</thinking>

<final diagnosis>Provide only the single most likely option without reasoning. If multiple options are plausible, always choose the most fine-grained (i.e., most specific or detailed) option available among them. Also provide the lesion condition (benign, malignant or precancerous in situ). </final diagnosis>

Ensure your response is medically accurate, concise, and strictly follows the specified format.

### Prompt template for disease diagnosis

**Question example** = What type of abnormality is present in this image? A: melanocytic nevus B: vascular lesion C: basal cell carcinoma D: squamous cell carcinoma

You are a medical vision-language assistant specializing in dermatology. Given the dermatology image, answer:

#### Question example

Provide necessary reasoning and only answer the question in the following format:

<thinking>Describe the key clinical features and visual observations that support your diagnosis.</thinking>

<final diagnosis>Provide only the single most likely option (A/B/C/D) without reasoning. If multiple options are plausible, always choose the most fine-grained (i.e., most specific or detailed) option available among them. </final diagnosis>

Ensure your response is medically accurate, concise, and strictly follows the specified format.

#### Prompt template for OOD diagnosis

**Question example** = What specific classification does this image fall under in terms of abnormality? A: Inflammatory. B: Traumatic C: Endocrine D: Infectious

You are a medical vision-language assistant specializing in dermatology. Given the dermatology image, answer:

**Question example**

Provide necessary reasoning and only answer the question in the following format:

<thinking>

Begin by describing the characteristic clinical features and visual observations of the lesion.

Based on these features, choose the most likely diagnosis from the options.

Then, identify at least one plausible alternative diagnosis from other options and describe its defining features.

Compare the observed lesion with these alternatives, and explain step by step why the final diagnosis is more consistent with the findings.

Conclude the reasoning with the single condition that best matches the clinical presentation.

</thinking>

<final diagnosis>Provide only the single most likely option without reasoning. </final diagnosis>

Ensure your response is medically accurate, concise, and strictly follows the specified format.

#### Prompt template for skin lesion diagnosis

You are a medical vision-language assistant specializing in dermatology.

Given the dermatology image, answer: What type of lesion condition (benign, malignant or precancerous in situ) is present in this image?

A: benign B: malignant C: precancerous in situ

Provide necessary reasoning and only answer the question in the following format:

<thinking>Describe the key clinical features and visual observations that support your diagnosis.</thinking>

<final diagnosis>Only output one option: A, B, or C.</final diagnosis>

Ensure your response is medically accurate, concise, and strictly follows the specified format.

#### Prompt template during evaluation for LLaVA-Med-7b

**Question example** = What specific classification does this image fall under in terms of abnormality? A: Inflammatory. B: Traumatic C: Endocrine D: Infectious

You are a medical vision-language assistant specializing in dermatology.

Given the dermatology image, answer: **Question example**

Give the correct option. Answer:

#### Prompt template during evaluation for SkinVL-PubMM

**Question example** = A: Inflammatory. B: Traumatic C: Endocrine D: Infectious

This is a skin lesion image. From the following categories: **Question example**

Which one is the diagnosis?

## E Qualitative Analysis

### Case 1

**Prompt** = You are a medical vision-language assistant specializing in dermatology. Given the dermatology image, answer: What type of abnormality is present in this image? Describe the key clinical features and visual observations that support your diagnosis. And then the diagnosis. Also provide the lesion condition (benign, malignant or precancerous in situ).



**Ground truth:** melanocytic nevus, benign

---

#### Response from Qwen2.5-VL-7B:

The image shows a skin surface with multiple fine hairs scattered across it. There is a distinct brownish patch on the skin, which appears slightly elevated and irregularly shaped.

##### Key Clinical Features and Visual Observations:

1. **Hair Growth**: The presence of fine hairs suggests that the area might be part of the scalp or another hairy region.
2. **Brownish Patch**: The central brownish patch is irregular in shape and has a slightly raised appearance compared to the surrounding skin. This could indicate a lesion.
3. **Color and Texture**: The color of the patch is not uniform, suggesting variability in pigmentation, which can be a sign of melanocytic activity or other skin changes.
4. **Elevation**: The patch appears slightly elevated, which could be indicative of a lesion such as a mole, nevus, or potentially a more concerning lesion like a melanoma.

##### ### Diagnosis:

Based on the clinical features observed, the most likely diagnosis is a **pigmented lesion**. The irregular shape, color variation, and slight elevation suggest that this could be a **mole** (nevus) or a **melanoma**. However, without a biopsy and further clinical evaluation by a dermatologist, it is impossible to definitively diagnose the nature of the lesion.

##### ### Lesion Condition:

Given the irregular shape, color variation, and slight elevation, the lesion cannot be classified as benign based on the image alone. It could be either benign (e.g., a common or atypical mole) or potentially malignant (e.g., a melanoma). Therefore, the lesion should be considered **precancerous in situ** until further evaluation by a dermatologist.

##### ### Recommendation:

It is crucial to consult a dermatologist for a proper evaluation. The dermatologist may perform a biopsy to determine the exact nature of the lesion and recommend appropriate treatment if necessary. Early detection and management of skin lesions are essential for preventing potential complications.

---

#### Response from Skin-R1:

The lesion exhibits the clinical features of melanocytic nevus, including a dark brown to black, sharply circumscribed macule with uniform color and no signs of asymmetry or irregular borders, indicating a benign pigmented nevus rather than melanoma. Therefore, the most likely diagnosis corresponds to "melanocytic nevus". The lesion is therefore classified as benign.

**Case 2**

**Prompt** = You are a medical vision-language assistant specializing in dermatology. Given the dermatology image, answer: What type of abnormality is present in this image? Describe the key clinical features and visual observations that support your diagnosis. And then the diagnosis. Also provide the lesion condition (benign, malignant or precancerous in situ).



**Ground truth:** basal cell carcinoma, malignant

**Response from Qwen2.5-VL-7B:**

The image shows a close-up view of skin with several key clinical features:

1. **Color Changes**: The skin appears to have areas of redness and some yellowish discoloration, which could indicate inflammation or infection.
2. **Lesion Appearance**: There is a small, irregularly shaped area of bright redness with a slightly raised border, suggesting an inflammatory process or a potential vascular issue.
3. **Surface Characteristics**: The surface of the lesion appears somewhat rough and possibly ulcerated, indicating a disruption in the normal skin barrier.

**### Key Clinical Features Supporting Diagnosis:**

- **Inflammatory Appearance**: The redness and surrounding changes suggest an inflammatory process.
- **Ulceration**: The presence of a small ulcer suggests a breakdown in the skin's integrity, which can be seen in various dermatological conditions such as infections, autoimmune diseases, or malignancies.

**### Diagnosis:**

Given the clinical features observed, the most likely diagnosis is **inflammatory dermatitis**. This is a broad term for a group of skin conditions characterized by inflammation. The specific type of dermatitis cannot be determined definitively from this image alone without further clinical history and examination.

**### Lesion Condition:**

Based on the appearance, the lesion is **benign**.

**Response from Skin-R1:**

The image shows ulceration with a well-defined, erythematous border and a central necrotic or crust-covered area, which may appear as a shallow or deep crater-like depression, indicating basal cell carcinoma. Therefore, the most likely diagnosis corresponds to basal cell carcinoma. The lesion is generally classified as malignant.

**Case 3**

**Prompt** = You are a medical vision-language assistant specializing in dermatology. Given the dermatology image, answer: What type of abnormality is present in this image? Describe the key clinical features and visual observations that support your diagnosis. And then the diagnosis. Also provide the lesion condition (benign, malignant or precancerous in situ).



**Ground truth:** melanoma, malignant

**Response from Qwen2.5-VL-7B:**

The provided image appears to be an abstract representation rather than a clear depiction of a skin lesion. However, based on the description of the image, it seems to show a complex pattern with irregular, wavy lines and areas of discoloration. This could potentially represent a variety of conditions depending on the context.

**### Key Clinical Features and Visual Observations:**

1. **\*\*Irregular Wavy Lines\*\*:** These could represent vascular structures, but without a clear view of the skin surface, it's difficult to determine their nature.
2. **\*\*Discoloration\*\*:** The presence of dark and light areas suggests possible pigmentation changes, which can be indicative of various dermatological conditions.
3. **\*\*Abstract Nature\*\*:** The lack of a clear lesion makes it challenging to provide a definitive diagnosis. This could be due to the image being abstract or a result of a specific imaging technique.

**### Diagnosis:**

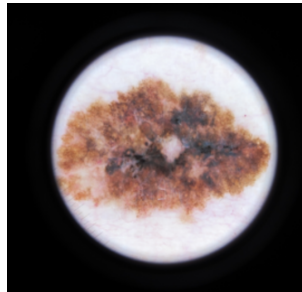
Given the abstract nature of the image, it is not possible to provide a precise diagnosis. However, if we were to speculate based on the visual cues, the image might resemble a dermoscopic image of a mole or a skin lesion with atypical features. The irregular lines and discoloration could suggest a premalignant or early-stage malignancy, such as a dysplastic nev...

**Response from Skin-R1:**

The lesion exhibits irregular borders with varying shades of brown, black, and tan, often showing asymmetry and multiple colors intermingled within the same lesion, which aligns with melanoma. Therefore, the most likely diagnosis corresponds to melanoma. The lesion is classified as malignant.

#### Case 4

**Prompt** = You are a medical vision-language assistant specializing in dermatology. Given the dermatology image, answer: What type of abnormality is present in this image? Describe the key clinical features and visual observations that support your diagnosis. And then the diagnosis. Also provide the lesion condition (benign, malignant or precancerous in situ).



**Ground truth:** melanoma, malignant

**Response from Qwen2.5-VL-7B:**

The image provided appears to be a dermoscopic view of a skin lesion. Here's an analysis based on the visual features:

**### Key Clinical Features and Observations:**

1. **Asymmetry**: The lesion does not appear symmetrical.
2. **Color Variability**: There is a mix of colors including brown, black, and reddish hues. The central area seems to have a darker, more irregular pigmentation.
3. **Irregular Borders**: The edges of the lesion are uneven and not well-defined.
4. **Structureless Reddish Area**: There is a reddish area with a structureless pattern, which can be concerning for malignancy.
5. **White/Gray Areas**: There are areas of white or gray, which could represent atrophy or depigmentation.

**### Diagnosis:**

Based on these dermoscopic features, the lesion exhibits characteristics that are often associated with melanoma. These include asymmetry, irregular borders, color variability, and the presence of a structureless red area, which is indicative of a junctional component.

**### Lesion Condition:**

Given the dermoscopic findings, this lesion is considered **malignant**. The presence of irregular borders, asymmetry, and the combination of colors are highly suggestive of...

**Response from Skin-R1:**

The lesion exhibits the clinical features of melanoma, including irregular borders, variable pigmentation, asymmetry, and changes in color with areas of dark brown, blue-gray, red, or gray-white, as well as a central tan to bluish-black macule surrounded by a hypopigmented halo, indicating subunit melanoma. Therefore, the most likely diagnosis corresponds to melanoma. The lesion is malignant.